

On Non-Negative Quadratic Programming in Geometric Optimization*

Siu-Wing Cheng[†]

Man Ting Wong[†]

Abstract

We present experimental and theoretical results on a method that applies a numerical solver iteratively to solve several non-negative quadratic programming problems in geometric optimization. The method gains efficiency by exploiting the potential sparsity of the intermediate solutions. We implemented the method to call `quadprog` of MATLAB iteratively. In comparison with a single call of `quadprog`, we obtain a 10-fold speedup on two proximity graph problems in \mathbb{R}^d on some public data sets, a 10-fold speedup on the minimum enclosing ball problem on random points in a unit cube in \mathbb{R}^d , and a 5-fold speedup on the polytope distance problem on random points from a cube in \mathbb{R}^d when the input size is significantly larger than the dimension; we also obtain a 2-fold or more speedup on deblurring some gray-scale space and thermal images via non-negative least square. We compare with two minimum enclosing ball software by Gärtner and Fischer et al.; for 1000 nearly cospherical points or random points in a unit cube, the iterative method overtakes the software by Gärtner at 20 dimensions and the software by Fischer et al. at 170 dimensions. In the image deblurring experiments, the iterative method compares favorably with other software that can solve non-negative least square, including FISTA with backtracking, SBB, FNNLS, and `lsqnonneg` of MATLAB. We analyze theoretically the number of iterations taken by the iterative scheme to reduce the gap between the current solution value and the optimum by a factor e . Under certain assumptions, we prove a bound proportional to the square root of the number of variables.

*Research supported by Research Grants Council, Hong Kong, China (project no. 16203718).

[†]Department of Computer Science and Engineering, HKUST, Hong Kong. Email: scheng@cse.ust.hk, mtwongaf@connect.ust.hk

1 Introduction

We study an iterative method to apply a numerical solver to solve *non-negative convex quadratic programming problems* (NNQ problems): $\min \mathbf{x}^t \mathbf{A}^t \mathbf{A} \mathbf{x} + \mathbf{a}^t \mathbf{x}$ subject to $\mathbf{B} \mathbf{x} \geq \mathbf{b}$, $\mathbf{C} \mathbf{x} = \mathbf{c}$, $\mathbf{x} \geq 0$. The method gains efficiency by exploiting the potential sparsity of the intermediate solutions. We study its performance both theoretically and experimentally on several NNQ problems that arise in geometric optimization.

The first problem is fitting a *proximity graph* to data points in \mathbb{R}^d , which finds applications in classification, regression, and clustering [19, 27, 28, 42]. Daitch et al. [19] defined a proximity graph via solving an NNQ problem. The unknown is a vector $\mathbf{x} \in \mathbb{R}^{n(n-1)/2}$, specifying the edge weights in the complete graph on the input points $\mathbf{p}_1, \dots, \mathbf{p}_n$. Let $(\mathbf{x})_{i\Delta j}$ denote the coordinate of \mathbf{x} that stores the weight of the edge $\mathbf{p}_i \mathbf{p}_j$. Edge weights must be non-negative; each point must have a total weight of at least 1 over its incident edges; these constraints can be modelled as $\mathbf{B} \mathbf{x} \geq \mathbf{1}_n$ and $\mathbf{x} \geq 0_{n(n-1)/2}$, where $\mathbf{B} \in \mathbb{R}^{n \times n(n-1)/2}$ is the incidence matrix for the complete graph, and $\mathbf{1}_n$ is the n -dimensional vector with all coordinates equal to 1. The objective is to minimize $\sum_{i=1}^n \left\| \sum_{j \in [n] \setminus \{i\}} (\mathbf{x})_{i\Delta j} (\mathbf{p}_i - \mathbf{p}_j) \right\|^2$, which can be written as $\mathbf{x}^t \mathbf{A}^t \mathbf{A} \mathbf{x}$ for some matrix $\mathbf{A} \in \mathbb{R}^{dn \times n(n-1)/2}$. We call this the DKSG problem. The one-dimensional case can be solved in $O(n^2)$ time [16].

We also study another proximity graph in \mathbb{R}^d defined by Zhang et al. [42] via minimizing $\frac{1}{d} \mathbf{b}^t \mathbf{x} + \frac{\mu}{2} \|\mathbf{U} \mathbf{x} - \mathbf{1}_n\|^2 + \frac{\rho}{2} \|\mathbf{x}\|^2$ for some constants $\mu, \rho \geq 0$. The vector $\mathbf{x} \in \mathbb{R}^{n(n-1)/2}$ stores the unknown edge weights. For all distinct $i, j \in [n]$, the coordinate $(\mathbf{b})_{i\Delta j}$ of \mathbf{b} is equal to $\|\mathbf{p}_i - \mathbf{p}_j\|^2$. The matrix \mathbf{U} is the incidence matrix for the complete graph. The objective function can be written as $\mathbf{x}^t \mathbf{A}^t \mathbf{A} \mathbf{x} + \mathbf{a}^t \mathbf{x}$, where $\mathbf{A}^t = \left[\frac{\mu}{2} \mathbf{U}^t \quad \frac{\rho}{2} \mathbf{I}_{n(n-1)/2} \right]$ and $\mathbf{a} = \frac{1}{d} \mathbf{b} - \mu \mathbf{U}^t \mathbf{1}_n$. The only constraints are $\mathbf{x} \geq 0_{n(n-1)/2}$. We call this the ZHLG problem.

The third problem is finding the minimum enclosing ball (MEB) of n points in \mathbb{R}^d [21, 23, 39]. It has connections to clustering [10, 14], computation of spatial hierarchies [26], and support vector machine research [12, 37, 38]. The approximate MEB problem is related to the study of coresets [13, 17, 30, 41]. Let $\mathbf{p}_1, \dots, \mathbf{p}_n$ be the input points. In the unknown vector $\mathbf{x} \in \mathbb{R}^n$, the coordinate $(\mathbf{x})_i$ stores the weight associated with \mathbf{p}_i in expressing the MEB center as a convex combination of the input points. The constraints are $\mathbf{1}_n^t \mathbf{x} = 1$ and $\mathbf{x} \geq 0_n$. The objective is to minimize $\mathbf{x}^t \mathbf{A}^t \mathbf{A} \mathbf{x} + \mathbf{a}^t \mathbf{x}$, where $\mathbf{A} = [\mathbf{p}_1 \ \dots \ \mathbf{p}_n]$ and $\mathbf{a} = [-\|\mathbf{p}_1\|^2 \ \dots \ -\|\mathbf{p}_n\|^2]^t$.

The fourth problem is to deblur some mildly sparse gray-scale images [25, 31]. The pixels in an image form a vector \mathbf{x} of gray scale values in \mathbb{R}^d ; the blurring can be modelled by the action of a matrix $\mathbf{A} \in \mathbb{R}^{d \times d}$ that depends on the particular point spread function adopted [31]; and $\mathbf{A} \mathbf{x}$ is the observed blurred image. Working backward, given the matrix \mathbf{A} and a blurred image \mathbf{b} , we recover the image by finding the unknown $\mathbf{x} \geq 0_d$ that minimizes $\|\mathbf{A} \mathbf{x} - \mathbf{b}\|^2$, which is a *non-negative least square problem* (NNLS) [29, 32]. The problem is often ill-posed, i.e., \mathbf{A} is not invertible.

The fifth problem is to find the distance between the convex hulls of two point sets in \mathbb{R}^d [24, 36, 40]. Wolfe [40] reported that the problem was encountered in the optimization of non-differentiable functions, approximation theory, and pattern recognition. We call it the PD problem. Due to space limitation, we defer the experimental results on the PD problem to Appendix D.4.

The method that we study selects a subset of variables as free variables—the non-free variables are fixed at zero—and calls the solver to solve a constrained NNQ in each iteration. It is reminiscent of the active-set method (e.g. [15, 18]) which determines a descent direction and an appropriate step size in that descent direction in each iteration. In contrast, our main task is selecting free variables; the descent step is carried out by calling a solver. A version of this method was used in [19] for solving the DKSG problem. However, it is only briefly mentioned that a small number of the most negative gradient coordinates are selected as free variables; no further details are given; there is no analysis of the convergence. We find the selection of free variables crucial. The right

answer is not some constant number of variables or a constant fraction of them. Also, one cannot always turn free variables that happen to be zero in an iteration into non-free variables in the next iteration as suggested in [19]; otherwise, the algorithm may not terminate in some cases.

We implemented the method to call `quadprog` of MATLAB iteratively. In comparison with a single call of `quadprog`, we obtain a 10-fold speedup on DKSG and ZHLG on some public data sets, a 10-fold speedup on MEB on random points in a unit cube, and a 5-fold speedup on PD on random points from a cube when the input size is significantly larger than the dimension; we also obtain a 2-fold or more speedup on deblurring some gray-scale space and thermal images via NNLS. We compare with two MEB software by Gärtner [22] and Fischer et al. [20]; for 1000 nearly cospherical points or random points in a unit cube, the iterative method overtakes the software by Gärtner at 20 dimensions and the software by Fischer et al. at 170 dimensions. In the image deblurring experiments, the iterative method compares favorably with other software that can solve NNLS, including FISTA with backtracking [5, 11], SBB [29], FNNLS [32], and `lsqnonneg` of MATLAB. We emphasize that we do not claim a solution for image deblurring as there are many issues that we do not address; we only seek to demonstrate the potential of the iterative scheme.

We use $f : \mathbb{R}^\nu \rightarrow \mathbb{R}$ to denote the objective function of the NNQ problem at hand. A unit direction $\mathbf{n} \in \mathbb{R}^\nu$ is a *descent direction* from a feasible solution \mathbf{x} if $\langle \nabla f(\mathbf{x}), \mathbf{n} \rangle < 0$ and $\mathbf{x} + s\mathbf{n}$ lies in the feasible region for some $s > 0$. We offer a partial theoretical analysis. Let \mathbf{x}_r be the solution produced in the $(r - 1)$ -th iteration. Let \mathbf{x}_* be the optimal solution. We prove that one can find a descent direction \mathbf{n}_r from \mathbf{x}_r , for which only a few variables need to be freed, such that if the distance between \mathbf{x}_r and the minimum in direction \mathbf{n}_r is assumed to be at least $\frac{1}{\lambda} \|\mathbf{x}_r - \mathbf{x}_*\|$ for all r , where λ is some value at least 1, then $f(\mathbf{x}_{r+i}) - f(\mathbf{x}_*) \leq e^{-1}(f(\mathbf{x}_r) - f(\mathbf{x}_*))$ for some $i = O(\lambda) \cdot$ square root of the number of variables. An intuitive interpretation is that even if the descent direction is far from ideal as we free only a few variables for the sake of efficiency, as long as we can move from the current solution by a sizable fraction of its distance from \mathbf{x}_* , a geometric-like convergence can be obtained. We checked this assumption in some of our experiments on DKSG and ZHLG; it is almost always satisfied for $\lambda = 10$ by the descent directions taken. Due to space limitation, the missing proofs can be found in the appendix.

We use uppercase and lowercase letters in typewriter font to denote matrices and vectors, respectively. Given a vector \mathbf{x} , we use $(\mathbf{x})_i$ to denote its i -th coordinate. The inner product of two vectors \mathbf{x} and \mathbf{y} is written as $\langle \mathbf{x}, \mathbf{y} \rangle$ or $\mathbf{x}^t \mathbf{y}$. The *span* of a set of vectors W is the linear subspace spanned by them, and we denote it by $\text{span}(W)$. In \mathbb{R}^ν , for $i \in [\nu]$, define the vector \mathbf{e}_i to have a value 1 in the i -th coordinate and zero at other coordinates. Given a set of vectors $\{\mathbf{w}_1, \mathbf{w}_2, \dots, \mathbf{w}_\nu\}$, a *conical combination* of them is $\sum_{i=1}^\nu c_i \mathbf{w}_i$ for some non-negative real values c_1, c_2, \dots, c_ν .

2 Algorithm

Figure 1(a) shows the NNQ problem *constrained by the active set* S_r that stores the non-free variables in the $(r - 1)$ -th iteration. Assume that $\mathbf{B} \in \mathbb{R}^{\kappa \times \nu}$. Let \mathbf{x}_r be the optimal solution of this constrained problem. Let \mathbf{u} and $\tilde{\mathbf{u}}$ be the vectors of Lagrange multipliers for the constraints $\mathbf{B}\mathbf{x} \geq \mathbf{b}$ and $\mathbf{C}\mathbf{x} = \mathbf{c}$, respectively. The coordinates of \mathbf{u} are required to be non-negative, whereas those of $\tilde{\mathbf{u}}$ are unrestricted. Let $\mathbf{v} \in \mathbb{R}^\nu$ be the vector of Lagrange multipliers for the constraints $\mathbf{x} \geq \mathbf{0}_\nu$. For each $i \in [\nu] \setminus S_r$, we require $(\mathbf{v})_i \geq 0$; for $i \in S_r$, $(\mathbf{v})_i$ is unrestricted. The dual of the constrained problem is shown in Figure 1(b), where $g(\mathbf{u}, \tilde{\mathbf{u}}, \mathbf{v}, \mathbf{x}) = f(\mathbf{x}) + \mathbf{u}^t(\mathbf{b} - \mathbf{B}\mathbf{x}) + \tilde{\mathbf{u}}^t(\mathbf{c} - \mathbf{C}\mathbf{x}) - \mathbf{v}^t \mathbf{x}$. In the dual, \mathbf{x} is unrestricted. Let $(\mathbf{u}_r, \tilde{\mathbf{u}}_r, \mathbf{v}_r, \mathbf{x}_r)$ be the optimal solution of g constrained by S_r . Let $\text{supp}(\mathbf{x}_r) = \{i \in [\nu] : (\mathbf{x}_r)_i \neq 0\}$. By optimality, the following KKT conditions must hold: (i) critical point: $\frac{\partial g}{\partial \mathbf{x}}(\mathbf{x}_r) = \nabla f(\mathbf{x}_r) - \mathbf{B}^t \mathbf{u}_r - \mathbf{C}^t \tilde{\mathbf{u}}_r - \mathbf{v}_r = \mathbf{0}_\nu$; (ii) primal feasibility: $\mathbf{B}\mathbf{x}_r \geq \mathbf{b}$, $\mathbf{C}\mathbf{x}_r = \mathbf{c}$, $(\mathbf{x}_r)_i = 0$

$$\begin{array}{ll}
\min & f(\mathbf{x}) \\
\text{s.t.} & \mathbf{B}\mathbf{x} \geq \mathbf{b}, \mathbf{C}\mathbf{x} = \mathbf{c}, \\
& \mathbf{x} \geq 0_\nu, \forall i \in S_r, (\mathbf{x})_i = 0. \\
& \text{(a) Constrained NNQ}
\end{array}
\qquad
\begin{array}{ll}
\max_{\mathbf{u}, \tilde{\mathbf{u}}, \mathbf{v}} & \min_{\mathbf{x}} g(\mathbf{u}, \tilde{\mathbf{u}}, \mathbf{v}, \mathbf{x}) \\
\text{s.t.} & \mathbf{u} \geq 0_\kappa, \\
& \forall i \notin S_r, (\mathbf{v})_i \geq 0. \\
& \text{(b) Dual of constrained NNQ}
\end{array}$$

Figure 1: The constrained NNQ and its dual.

for $i \in S_r$, and $\mathbf{x}_r \geq 0_\nu$; (iii) dual feasibility: $\mathbf{u}_r \geq 0_\kappa$, $(\mathbf{v}_r)_i \geq 0$ for $i \in [\nu] \setminus S_r$; (iv) complementary slackness: $(\mathbf{u}_r)_i \cdot (\mathbf{b} - \mathbf{B}\mathbf{x}_r)_i = 0$ for $i \in [\kappa]$, and $(\mathbf{v}_r)_i \cdot (\mathbf{x}_r)_i = 0$ for $i \in [\nu]$.

For efficiency, before computing \mathbf{x}_r in the previous iteration, we eliminated the variables corresponding to the coordinates of \mathbf{x}_r that belong to S_r . So the solver cannot return all Lagrange multipliers encoded in \mathbf{v}_r ; nevertheless, as long as the solver returns \mathbf{u}_r , $\tilde{\mathbf{u}}_r$, and \mathbf{x}_r , we can compute \mathbf{v}_r using the first KKT condition. Thus, an optimal solution of the dual constrained by S_r is fully characterized by $(\mathbf{u}_r, \tilde{\mathbf{u}}_r, \mathbf{x}_r)$. By strong duality, the optimum of g constrained by S_r is equal to the optimum of f constrained by S_r . If \mathbf{x}_r is not an optimal solution, there must exist some $j \in S_r$ such that if j is removed from S_r , then $(\mathbf{u}_r, \tilde{\mathbf{u}}_r, \mathbf{x}_r)$ is non-optimal with respect to the updated active set. Among the KKT conditions, only the dual feasibility can be violated by removing j from S_r ; in case of violation, we must have $(\mathbf{v}_r)_j < 0$. For each $i \in S_r$, we check whether $(\mathbf{v}_r)_i < 0$, or equivalently, $(\nabla f(\mathbf{x}_r) - \mathbf{B}^t \mathbf{u}_r - \mathbf{C}^t \tilde{\mathbf{u}}_r)_i < 0$. We select a subset of the negative coordinates of $\nabla f(\mathbf{x}_r) - \mathbf{B}^t \mathbf{u}_r - \mathbf{C}^t \tilde{\mathbf{u}}_r$ to update the active set. SolveNNQ in Algorithm 1 describes the iterative method.

Algorithm 1 SolveNNQ

```

1:  $\tau$  is an integer threshold much less than  $\nu$ 
2:  $\beta_0$  is a threshold on  $|E_r|$  such that  $\beta_0 > \tau$ 
3:  $\beta_1$  is a threshold on the number of iterations
4: compute an initial active set  $S_1$  and an optimal solution  $(\mathbf{u}_1, \tilde{\mathbf{u}}_1, \mathbf{x}_1)$  of  $g$  constrained by  $S_1$ 
5:  $r \leftarrow 1$ 
6: loop
7:    $E_r \leftarrow$  the sequence of indices  $i \in S_r$  such that  $(\mathbf{v}_r)_i = (\nabla f(\mathbf{x}_r) - \mathbf{B}^t \mathbf{u}_r - \mathbf{C}^t \tilde{\mathbf{u}}_r)_i < 0$  and  $E_r$  is
   sorted in non-decreasing order of  $(\mathbf{v}_r)_i$ 
8:   if  $E_r = \emptyset$  then
9:     return  $\mathbf{x}_r$ 
10:  else
11:    if  $|E_r| < \beta_0$  or  $r > \beta_1$  then
12:       $S_{r+1} \leftarrow S_r \setminus E_r$ 
13:    else
14:      let  $E'_r$  be subset of the first  $\tau$  indices in  $E_r$ 
15:       $S_{r+1} \leftarrow [\nu] \setminus (\text{supp}(\mathbf{x}_r) \cup E'_r)$ 
16:    end if
17:  end if
18:   $(\mathbf{u}_{r+1}, \tilde{\mathbf{u}}_{r+1}, \mathbf{x}_{r+1}) \leftarrow$  optimal solution of  $g$  constrained by the active set  $S_{r+1}$ 
19:   $r \leftarrow r + 1$ 
20: end loop

```

In line 15 of SolveNNQ, we kick out all free variables that are zero in the current solution \mathbf{x}_r , i.e., if $i \notin S_r$ and $i \notin \text{supp}(\mathbf{x}_r)$, move i to S_{r+1} . This step keeps the number of free variables small so that the next call of the solver will run fast. When the computation is near its end, moving

a free variable wrongly to the active set can be costly; it is preferable to shrink the active set to stay on course for the optimal solution \mathbf{x}_* . Therefore, we have a threshold β_0 on $|E_r|$ and set $S_{r+1} := S_r \setminus E_r$ in line 12 if $|E_r| < \beta_0$. The threshold β_0 gives us control on the number of free variables. In some rare cases when we are near \mathbf{x}_* , the algorithm may alternate between excluding a primal variable from the active set in one iteration and moving the same variable into the active set in the next iteration. The algorithm may not terminate. Therefore, we have another threshold β_1 on the number of iterations beyond which the active set will be shrunk monotonically in line 12, thereby guaranteeing convergence. We will see later that if β_1 is not exceeded, the iterations of lines 7–19 converge quickly to the optimum under some assumption. If β_1 is exceeded, we can still bound the number of remaining iterations by $|\text{supp}(\mathbf{x}_*)|$ (see Appendix A.1), but we will have no control on the number of free variables. The threshold β_1 is rarely exceeded in our experiments; setting $S_{r+1} := S_r \setminus E_r$ when $|E_r| < \beta_0$ also helps to keep the the algorithm from exceeding the threshold β_1 . In our experiments, we set $\tau = \Theta(\log^2 \nu)$, $\beta_0 = \Theta(\tau)$, and β_1 to be a constant; more details are given in Section 5.

Lemma 2.1. *Let $\mathbf{n} \in \mathbb{R}^\nu$ be any unit descent direction from \mathbf{x}_r . Let $\mathbf{y} = \mathbf{x}_r + \alpha \mathbf{n}$ for some $\alpha > 0$ be the feasible point that minimizes f on the ray from \mathbf{x}_r in direction \mathbf{n} . Then, (i) $f(\mathbf{x}_r) - f(\mathbf{y}) \leq -\|\mathbf{x}_r - \mathbf{y}\| \cdot \langle \nabla f(\mathbf{x}_r), \mathbf{n} \rangle$, and (ii) $f(\mathbf{x}_r) - f(\mathbf{y}) \geq -\frac{1}{2}\|\mathbf{x}_r - \mathbf{y}\| \cdot \langle \nabla f(\mathbf{x}_r), \mathbf{n} \rangle$.*

Corollary 2.1. *Let $\mathbf{n} \in \mathbb{R}^\nu$ be any unit descent direction from \mathbf{x}_r . Let $\mathbf{y} = \mathbf{x}_r + \alpha \mathbf{n}$ for some $\alpha > 0$ be the feasible point that minimizes f on the ray from \mathbf{x}_r in direction \mathbf{n} . Let S be an active set that is disjoint from $\text{supp}(\mathbf{x}_r) \cup \text{supp}(\mathbf{n})$. Let \mathbf{x}_{r+1} be the optimal solution for f constrained by S . Then, $\frac{f(\mathbf{x}_r) - f(\mathbf{x}_{r+1})}{f(\mathbf{x}_r) - f(\mathbf{x}_*)} \geq \frac{f(\mathbf{x}_r) - f(\mathbf{y})}{f(\mathbf{x}_r) - f(\mathbf{x}_*)} \geq \frac{\|\mathbf{x}_r - \mathbf{y}\|}{2} \cdot \frac{\langle \nabla f(\mathbf{x}_r), \mathbf{n} \rangle}{\langle \nabla f(\mathbf{x}_r), \mathbf{x}_* - \mathbf{x}_r \rangle}$.*

3 Convergence analysis for NNLS and ZHLG

Let L be an affine subspace in \mathbb{R}^ν . For every $\mathbf{x} \in \mathbb{R}^\nu$, define $\mathbf{x} \downarrow L$ to be the projection of \mathbf{x} to the linear subspace parallel to L —the translate of L that contains the origin. Note that $\mathbf{x} \downarrow L$ may not belong to L ; it does if L is a linear subspace. One can verify that $(-\mathbf{x}) \downarrow L = -(\mathbf{x} \downarrow L)$, so we will write $-\mathbf{x} \downarrow L$ without any bracket. In the pseudocode of SolveNNQ, E_r is a sequence of indices $i \in S_r$ such that $(\mathbf{v}_r)_i < 0$, arranged in non-decreasing order of $(\mathbf{v}_r)_i$. Define $J_r = \text{span}(\{\mathbf{e}_i : i \in E_r\})$. Lemma 3.1 below states a key result that the first τ indices in E_r induce a conical combination that is a good descent direction. We give the analysis in Appendix B.

Lemma 3.1. *The vectors in $\{\mathbf{e}_i : i \text{ among the first } \tau \text{ indices in } E_r\}$ have a unit conical combination \mathbf{n}_r such that \mathbf{n}_r is a descent direction from \mathbf{x}_r and $\angle(-\mathbf{v}_r \downarrow J_r, \mathbf{n}_r) \leq \arccos(\sqrt{\alpha/(2 \ln \nu)})$, where $\alpha = \min\{1, \tau/|E_r|\}$.*

We use Lemma 3.1 to establish a convergence rate under an assumption.

Lemma 3.2. *Let \mathbf{n}_r be a unit descent direction from \mathbf{x}_r that satisfies Lemma 3.1. Let \mathbf{y}_r be the feasible point that minimizes f on the ray from \mathbf{x}_r in direction \mathbf{n}_r . Let $\alpha = \min\{1, \tau/|E_r|\}$. If there exists λ such that $\|\mathbf{x}_r - \mathbf{y}_r\| \geq \frac{1}{\lambda}\|\mathbf{x}_r - \mathbf{x}_*\|$, then $\frac{f(\mathbf{x}_{r+1}) - f(\mathbf{x}_*)}{f(\mathbf{x}_r) - f(\mathbf{x}_*)} \leq 1 - \frac{1}{2\lambda\sqrt{2 \ln \nu/\alpha}}$.*

Proof. Irrespective of whether S_{r+1} is computed in line 12 or 15 of SolveNNQ, S_{r+1} is disjoint from $\text{supp}(\mathbf{x}_r) \cup \text{supp}(\mathbf{n}_r)$, which makes Corollary 2.1 applicable.

Since $\nabla f(\mathbf{x}_r) = \mathbf{v}_r$ for an NNLS or ZHLG problem, we have $\langle -\nabla f(\mathbf{x}_r), \mathbf{n}_r \rangle = \langle -\mathbf{v}_r, \mathbf{n}_r \rangle = \langle -\mathbf{v}_r \downarrow J_r, \mathbf{n}_r \rangle$. The last equality comes from the fact that $\mathbf{n}_r \in J_r$, so the component of $-\mathbf{v}_r$ orthogonal to J_r vanishes in the inner product. By Lemma 3.1, $\langle -\nabla f(\mathbf{x}_r), \mathbf{n}_r \rangle = \langle -\mathbf{v}_r \downarrow J_r, \mathbf{n}_r \rangle = \|\mathbf{v}_r \downarrow J_r\| \cdot \cos \angle(-\mathbf{v}_r \downarrow J_r, \mathbf{n}_r) \geq \|\mathbf{v}_r \downarrow J_r\| \cdot \frac{1}{\sqrt{2 \ln \nu/\alpha}}$.

The inequality above takes care of the nominator in the bound in Corollary 2.1 multiplied by -1 . The denominator in the bound in Corollary 2.1 multiplied by -1 is equal to $\langle -\nabla f(\mathbf{x}_r), \mathbf{x}_* - \mathbf{x}_r \rangle = \langle -\mathbf{v}_r, \mathbf{x}_* - \mathbf{x}_r \rangle = \langle -\mathbf{v}_r \downarrow J_r, \mathbf{x}_* - \mathbf{x}_r \rangle + \langle -\mathbf{v}_r + \mathbf{v}_r \downarrow J_r, \mathbf{x}_* - \mathbf{x}_r \rangle$.

Recall that $(\mathbf{v}_r \downarrow J_r)_i$ is $(\mathbf{v}_r)_i$ for $i \in E_r$ and zero otherwise. Therefore, $(-\mathbf{v}_r + \mathbf{v}_r \downarrow J_r)_i$ is zero for $i \in E_r$ and $-(\mathbf{v}_r)_i$ otherwise. If $i \notin E_r$, then $(\mathbf{v}_r)_i \geq 0$, which implies that $(-\mathbf{v}_r + \mathbf{v}_r \downarrow J_r)_i = -(\mathbf{v}_r)_i \leq 0$. By the complementary slackness, if $(\mathbf{v}_r)_i > 0$, then $(\mathbf{x}_r)_i = 0$, which implies that $(\mathbf{x}_* - \mathbf{x}_r)_i \geq 0$ as \mathbf{x}_* is non-negative. Altogether, we conclude that for $i \in [\nu]$, if $i \in E_r$ or $(i \notin E_r \wedge (\mathbf{v}_r)_i = 0)$, then $(-\mathbf{v}_r + \mathbf{v}_r \downarrow J_r)_i \cdot (\mathbf{x}_* - \mathbf{x}_r)_i = 0$; otherwise, $(-\mathbf{v}_r + \mathbf{v}_r \downarrow J_r)_i \cdot (\mathbf{x}_* - \mathbf{x}_r)_i \leq 0$. Therefore, $\langle -\mathbf{v}_r + \mathbf{v}_r \downarrow J_r, \mathbf{x}_* - \mathbf{x}_r \rangle \leq 0$. As a result, $\langle -\nabla f(\mathbf{x}_r), \mathbf{x}_* - \mathbf{x}_r \rangle \leq \langle -\mathbf{v}_r \downarrow J_r, \mathbf{x}_* - \mathbf{x}_r \rangle \leq \|\mathbf{x}_* - \mathbf{x}_r\| \cdot \|\mathbf{v}_r \downarrow J_r\|$.

Substituting the results in the above into Corollary 2.1 gives $\frac{f(\mathbf{x}_r) - f(\mathbf{x}_{r+1})}{f(\mathbf{x}_r) - f(\mathbf{x}_*)} \geq \frac{\|\mathbf{x}_r - \mathbf{y}_r\|}{2\|\mathbf{x}_* - \mathbf{x}_r\|} \cdot \frac{1}{\sqrt{2 \ln \nu / \alpha}}$. It then follows from the assumption of $\|\mathbf{x}_r - \mathbf{y}_r\| \geq \frac{1}{\lambda} \|\mathbf{x}_r - \mathbf{x}_*\|$ in the lemma that $f(\mathbf{x}_{r+1}) - f(\mathbf{x}_*) = (f(\mathbf{x}_r) - f(\mathbf{x}_*)) - (f(\mathbf{x}_r) - f(\mathbf{x}_{r+1})) \leq (f(\mathbf{x}_r) - f(\mathbf{x}_*)) - \frac{1}{2\lambda\sqrt{2 \ln \nu / \alpha}} (f(\mathbf{x}_r) - f(\mathbf{x}_*))$. \square

Let $T(v)$ be the time complexity of solving a convex quadratic program with v variables, assuming that the number of constraints is $O(v)$. It is known that $T(v) = O(v^3)$ [35]. Theorem 3.1 below follows from Lemma 3.2; the running time is analyzed in Appendix B.2.

Theorem 3.1. *Consider the application of SolveNNQ on an NNLS problem with n constraints in \mathbb{R}^d or a ZHLG problem for n points in \mathbb{R}^d . Let ν be n for NNLS or $n(n-1)/2$ for ZHLG. The initialization of SolveNNQ can be done in $T(\beta_0) + O(dn^2)$ time for NNLS or $T(\beta_0) + O(n^4)$ time for ZHLG. Suppose that the threshold β_1 on the total number of iterations is not exceeded, and there exists λ such that $\|\mathbf{x}_r - \mathbf{y}_r\| \geq \frac{1}{\lambda} \|\mathbf{x}_r - \mathbf{x}_*\|$ for all $r \geq 1$, where \mathbf{y}_r is the feasible point that minimizes f on the ray from \mathbf{x}_r in the descent direction that satisfies Lemma 3.1. Then, for all $r \geq 1$, $f(\mathbf{x}_{r+i}) - f(\mathbf{x}_*) \leq e^{-1} (f(\mathbf{x}_r) - f(\mathbf{x}_*))$ for some $i = O(\lambda\sqrt{\nu \log \nu / \tau})$, and each iteration in SolveNNQ takes $T(k + \beta_0) + O(k\nu + \beta_0^2)$ time, where $k = \max_{r \geq 1} |\text{supp}(\mathbf{x}_r)|$.*

For ease of presentation, we assume in Theorem 3.1 that $\|\mathbf{x}_r - \mathbf{y}_r\| \geq \frac{1}{\lambda} \|\mathbf{x}_r - \mathbf{x}_*\|$ for all $r \geq 1$; nevertheless, the gap $f(\mathbf{x}_r) - f(\mathbf{x}_*)$ will still decrease by a factor e after $O(\lambda\sqrt{\nu \log \nu / \tau})$ not necessarily consecutive iterations in the future that satisfy the assumption.

4 Convergence analysis for MEB, PD, and DKSG

We first present some general results; they will be specialized to MEB, PD, and DKSG. Suppose that the feasible region is described by a system of equality constraints $\mathbf{M}\mathbf{x} = \mathbf{m}$ for some matrix $\mathbf{M} \in \mathbb{R}^{\kappa \times \nu}$ and vector $\mathbf{m} \in \mathbb{R}^\kappa$, in addition to the constraints $\mathbf{x} \geq 0_\nu$. We use $(\mathbf{M})_{a,i}$ to denote the entry at the a -th row and i -th column. Recall that $(\tilde{\mathbf{u}}_r, \mathbf{v}_r, \mathbf{x}_r)$ form the solution of the dual problem constrained by the active set S_r , where $\tilde{\mathbf{u}}_r$ are the dual variables corresponding to the constraints $\mathbf{M}\mathbf{x} = \mathbf{m}$. For $a \in [\kappa]$, the a -th constraint is a hyperplane in \mathbb{R}^ν with $[(\mathbf{M})_{a,1} \ \dots \ (\mathbf{M})_{a,\nu}]^t$ as a normal vector. As a result, for any direction \mathbf{k} from the current solution \mathbf{x}_r that is parallel to the hyperplanes encoded by $\mathbf{M}\mathbf{x} = \mathbf{m}$, the vector $\mathbf{M}^t \tilde{\mathbf{u}}_r$ is orthogonal to \mathbf{k} , which gives

$$\langle \nabla f(\mathbf{x}_r), \mathbf{k} \rangle = \langle \nabla f(\mathbf{x}_r) - \mathbf{M}^t \tilde{\mathbf{u}}_r, \mathbf{k} \rangle = \langle \mathbf{v}_r, \mathbf{k} \rangle.$$

Without loss of generality, assume that $(\mathbf{v}_r)_1 = \min_{i \in E_r} (\mathbf{v}_r)_i$. Define the following items:

$$K_r = \{\mathbf{x} \in \mathbb{R}^\nu : \forall i \notin E_r \cup \text{supp}(\mathbf{x}_r), (\mathbf{x})_i = 0\}, \quad \forall a \in [\kappa], I_a = \text{supp}(\mathbf{x}_r) \cap \{i : (\mathbf{M})_{a,i} \neq 0\},$$

$$\forall a \in [\kappa], H_a = \left\{ \mathbf{x} \in \mathbb{R}^\nu : \sum_{i \in \{1\} \cup I_a} (\mathbf{M})_{a,i} (\mathbf{x})_i = (\mathbf{m})_a \wedge \forall i \notin \{1\} \cup \text{supp}(\mathbf{x}_r), (\mathbf{x})_i = 0 \right\},$$

$$h = \bigcap_{a \in [\kappa]} H_a, \quad \forall a \in [\kappa], \forall i \in [\nu], (\mathbf{k}_a)_i = \begin{cases} \frac{(\mathbf{M})_{a,i}}{\sqrt{\sum_{j \in \{1\} \cup I_a} (\mathbf{M})_{a,j}^2}} & \text{if } i \in \{1\} \cup I_a, \\ 0 & \text{otherwise.} \end{cases}$$

For $a \in [\kappa]$, $1 \notin I_a$ as $I_a \subseteq \text{supp}(\mathbf{x}_r)$ and $1 \in E_r$. For $a \in [\kappa]$, H_a is an affine subspace of the a -th hyperplane in $\mathbf{M}\mathbf{x} = \mathbf{m}$. The solution \mathbf{x}_r lies in h . For $a \in [\kappa]$, \mathbf{k}_a is a unit vector normal to H_a . Each H_a is a hyperplane in $\text{span}(\{\mathbf{e}_i : i \in \{1\} \cup \text{supp}(\mathbf{x}_r)\})$. So h has dimension $|\text{supp}(\mathbf{x}_r)| + 1 - \kappa$. We assume that $|\text{supp}(\mathbf{x}_r)| + 1 - \kappa$ is positive which will be the case for MEB, PD, and DKSG. The subspace of $\text{span}(\{\mathbf{e}_i : i \in \{1\} \cup \text{supp}(\mathbf{x}_r)\})$ orthogonal to h is κ -dimensional, and it is equal to $\text{span}(\{\mathbf{k}_a : a \in [\kappa]\})$. The following equalities follow easily:

$$\begin{aligned} \mathbf{e}_1 \downarrow h &= \mathbf{e}_1 - \sum_{a \in [\kappa]} \langle \mathbf{e}_1, \mathbf{k}_a \rangle \mathbf{k}_a = \mathbf{e}_1 - \sum_{a \in [\kappa]} \frac{(\mathbf{M})_{a,1}}{\sqrt{\sum_{j \in \{1\} \cup I_a} (\mathbf{M})_{a,j}^2}} \cdot \mathbf{k}_a. \\ \langle \mathbf{v}_r \downarrow K_r, \mathbf{e}_1 \downarrow h \rangle &= \langle \mathbf{v}_r \downarrow K_r, \mathbf{e}_1 \rangle - \sum_{a \in [\kappa]} \frac{(\mathbf{M})_{a,1}}{\sqrt{\sum_{j \in \{1\} \cup I_a} (\mathbf{M})_{a,j}^2}} \cdot \langle \mathbf{v}_r \downarrow K_r, \mathbf{k}_a \rangle. \end{aligned}$$

Lemma 4.1 shows that freeing the variable $(\mathbf{x})_1$ admits a good descent direction; we can show that $\langle \mathbf{v}_r \downarrow K_r, \mathbf{e}_1 \downarrow h \rangle < 0$ for MEB, PD, and DKSG. Combining Lemmas 4.1 and 4.2 shows a geometric-like convergence under the assumption that the distance between \mathbf{x}_r and the minimum in the descent direction that frees \mathbf{x}_1 is at least $\frac{1}{\lambda} \|\mathbf{x}_r - \mathbf{x}_*\|$.

Lemma 4.1. *Let S be an active set disjoint from $\{1\} \cup \text{supp}(\mathbf{x}_r)$. If $\langle \mathbf{v}_r \downarrow K_r, \mathbf{e}_1 \downarrow h \rangle < 0$, then $\mathbf{n}_r = \mathbf{e}_1 \downarrow h / \|\mathbf{e}_1 \downarrow h\|$ is a unit descent direction from \mathbf{x}_r with respect to S and $\cos \angle(-\mathbf{v}_r \downarrow K_r, \mathbf{n}_r) \geq \langle -\mathbf{v}_r \downarrow K_r, \mathbf{e}_1 \downarrow h \rangle \cdot \|\mathbf{v}_r \downarrow K_r\|^{-1}$.*

Lemma 4.2. *Suppose that there exist positive λ and γ such that $\cos \angle(-\mathbf{v}_r \downarrow K_r, \mathbf{n}_r) \geq 1/\gamma$ and $\|\mathbf{x}_r - \mathbf{y}_r\| \geq \frac{1}{\lambda} \|\mathbf{x}_r - \mathbf{x}_*\|$ for all $r \geq 1$, where \mathbf{n}_r is the unit descent direction that satisfies Lemma 4.1 with respect to the active set S_{r+1} , and \mathbf{y}_r is the feasible point that minimizes f on the ray from \mathbf{x}_r in direction \mathbf{n}_r . Then, for all $r \geq 1$, $f(\mathbf{x}_{r+i}) - f(\mathbf{x}_*) \leq e^{-1}(f(\mathbf{x}_r) - f(\mathbf{x}_*))$ for some $i \leq 2\lambda\gamma$.*

MEB. The hyperplane $\{\mathbf{x} \in \mathbb{R}^n : \sum_{i=1}^n (\mathbf{x})_i = 1\}$ contains all feasible solution. We have $[\kappa] = \{1\}$; $I_1 = \text{supp}(\mathbf{x}_r)$; $(\mathbf{M})_{1,i} = 1$ for $i \in [n]$. As $|\text{supp}(\mathbf{x}_r)| \geq 1$, $\frac{(\mathbf{M})_{1,1}^2}{\sum_{i \in \{1\} \cup I_1} (\mathbf{M})_{1,i}^2} = \frac{1}{|\text{supp}(\mathbf{x}_r)|+1} \leq \frac{1}{2}$. Thus, $\langle \mathbf{v}_r \downarrow K_r, \mathbf{e}_1 \downarrow h \rangle = (\mathbf{v}_r)_1 - \frac{1}{\sqrt{|\text{supp}(\mathbf{x}_r)|+1}} \langle \mathbf{v}_r \downarrow K_r, \mathbf{k}_1 \rangle$. For $i \notin \{1\} \cup \text{supp}(\mathbf{x}_r)$, $(\mathbf{k}_1)_i = 0$. For $i \in \{1\} \cup \text{supp}(\mathbf{x}_r)$, $(\mathbf{k}_1)_i = \frac{1}{\sqrt{|\text{supp}(\mathbf{x}_r)|+1}}$. By complementary slackness, for all $i \in \text{supp}(\mathbf{x}_r)$, $(\mathbf{v}_r)_i = 0$ as $(\mathbf{x}_r)_i > 0$. Thus, $\langle \mathbf{v}_r \downarrow K_r, \mathbf{k}_1 \rangle = (\mathbf{v}_r)_1 \cdot (\mathbf{k}_1)_1 = \frac{1}{\sqrt{|\text{supp}(\mathbf{x}_r)|+1}} (\mathbf{v}_r)_1$ and $\langle \mathbf{v}_r \downarrow K_r, \mathbf{e}_1 \downarrow h \rangle = (\mathbf{v}_r)_1 \cdot \left(1 - \frac{1}{|\text{supp}(\mathbf{x}_r)|+1}\right) \leq \frac{1}{2} (\mathbf{v}_r)_1 < 0$. Since $(\mathbf{v}_r)_i = 0$ for $i \in \text{supp}(\mathbf{x}_r)$, we have $\|\mathbf{v}_r \downarrow K_r\|^2 = \sum_{i \in E_r} (\mathbf{v}_r)_i^2 \leq |E_r| \cdot (\mathbf{v}_r)_1^2$. By Lemma 4.1, $\cos \angle(-\mathbf{v}_r \downarrow K_r, \mathbf{n}_r) \geq 1/\sqrt{2|E_r|} \geq 1/\sqrt{2n}$. Then, Lemma 4.2 implies that SolveNNQ reduces $f(\mathbf{x}_r) - f(\mathbf{x}_*)$ by a factor e in $O(\lambda\sqrt{n})$ iterations.

PD. Let the two input point sets be $\{\mathbf{p}_1, \dots, \mathbf{p}_m\}$ and $\{\mathbf{q}_1, \dots, \mathbf{q}_n\}$. Every feasible solution lies in the following two hyperplanes: $\sum_{i=1}^m (\mathbf{x})_i = 1$ and $\sum_{i=m+1}^{m+n} (\mathbf{x})_i = 1$. We have $[\kappa] = \{1, 2\}$; $I_1 = \text{supp}(\mathbf{x}_r) \cap [m]$; $(\mathbf{M})_{1,i} = 1$ for all $i \in \{1\} \cup I_1$. Thus, $\frac{(\mathbf{M})_{1,1}^2}{\sum_{i \in \{1\} \cup I_1} (\mathbf{M})_{1,i}^2} = \frac{1}{|I_1|+1} \leq \frac{1}{2}$. We have $(\mathbf{v}_r \downarrow K_r)_1 = (\mathbf{v}_r)_1$. Thus, $\langle \mathbf{v}_r \downarrow K_r, \mathbf{e}_1 \downarrow h \rangle = (\mathbf{v}_r)_1 - \frac{1}{\sqrt{|I_1|+1}} \langle \mathbf{v}_r \downarrow K_r, \mathbf{k}_1 \rangle$. As in the case of MEB, $\cos \angle(-\mathbf{v}_r \downarrow K_r, \mathbf{n}_r) \geq 1/\sqrt{2|E_r|} \geq 1/\sqrt{2(m+n)}$. So Lemma 4.2 implies that SolveNNQ reduces $f(\mathbf{x}_r) - f(\mathbf{x}_*)$ by a factor e in $O(\lambda\sqrt{m+n})$ iterations.

DKSG. We follow the approach in the analysis for MEB. To do so, we transform the inequality constraints to equality constraints by introducing n slack variables. The details are in Appendix C.2. The conclusion is that SolveNNQ reduces $f(\mathbf{x}_r) - f(\mathbf{x}_*)$ by a factor e in $O(\lambda n)$ iterations.

Theorem 4.1. *Consider running SolveNNQ on an MEB, PD, or DKSG problem. Let $k = \max_{r \geq 1} |\text{supp}(\mathbf{x}_r)|$. For all $r \geq 1$, there is a unit descent direction \mathbf{n}_r from \mathbf{x}_r that satisfies Lemma 4.1 so that $\cos \angle(-\mathbf{v}_r \downarrow K_r, \mathbf{n}_r) \geq 1/\gamma$, where γ is $\Theta(\sqrt{n})$ for MEB, $\Theta(\sqrt{m+n})$ for PD, and $\Theta(n)$ for DKSG. Suppose that the threshold β_1 on the number of iterations is not exceeded, and that $\|\mathbf{x}_r - \mathbf{y}_r\| \geq \frac{1}{\lambda} \|\mathbf{x}_r - \mathbf{x}_*\|$ for all $r \geq 1$, where \mathbf{y}_r is the feasible point that minimizes f on the ray from \mathbf{x}_r in direction \mathbf{n}_r .*

- MEB: Initialization takes $T(d+1) + O(dn^2)$ time. For $r \geq 1$, $f(\mathbf{x}_{r+i}) - f(\mathbf{x}_*) \leq e^{-1}(f(\mathbf{x}_r) - f(\mathbf{x}_*))$ for some $i = O(\lambda\sqrt{n})$. Each iteration takes $T(k + \beta_0) + O(kn + \beta_0^2)$ time.
- PD: Initialization takes $O(dm^2 + dn^2)$ time. For $r \geq 1$, $f(\mathbf{x}_{r+i}) - f(\mathbf{x}_*) \leq e^{-1}(f(\mathbf{x}_r) - f(\mathbf{x}_*))$ for some $i = O(\lambda\sqrt{m+n})$. Each iteration takes $T(k + \beta_0) + O(km + kn + \beta_0^2)$ time.
- DKSG: Initialization takes $T(n + \beta_0 - 1) + O(dn^4 + \beta_0^2)$ time. For $r \geq 1$, $f(\mathbf{x}_{r+i}) - f(\mathbf{x}_*) \leq e^{-1}(f(\mathbf{x}_r) - f(\mathbf{x}_*))$ for some $i = O(\lambda n)$. Each iteration takes $T(k + \beta_0) + O(kn^2 + \beta_0^2)$ time.

As discussed in the case of Theorem 3.1, the gap $f(\mathbf{x}_r) - f(\mathbf{x}_*)$ for MEB, PD, and DKSG will still reduce by a factor e after $O(\lambda\gamma)$ not necessarily consecutive iterations in the future that satisfy the assumption.

5 Experimental results

Our machine configuration is: Intel Core 7-9700K 3.6Hz cpu, 3600 Mhz ram, 8 cores, 8 logical processors. We use MATLAB version R2020b. We use the version of `quadprog` that runs the interior-point-convex algorithm. In each iteration, we should extract the submatrices corresponding to the free variables; however, doing so incurs a large amount of data movements. Instead, we zero out the rows and columns corresponding to the variables in the active set. We determine that $\tau = 4 \ln^2 \nu$ is a good setting for the DKSG and ZHLG data sets. We set $\tau = 4 \ln^2 \nu$ in the experiments with MEB, image deblurring, and PD as well without checking whether this is the best for them. It helps to verify the robustness of this choice of τ . We set β_0 to be 3τ and β_1 to be 15. Due to space limitation, the experimental results that show that SolveNNQ often achieves a 5-fold speedup over a single call of `quadprog` on PD are deferred to Appendix D.4.

5.1 DKSG and ZHLG

We set $\mu = 16$ and $\rho = 2$ in the objective function for ZHLG which are good settings according to [42]. We experimented with the data sets Iris, HCV, Ionosphere, and AAL [9]. For each data set, we sampled a number of rows that represent the number of points n and a number of attributes that represent the number of dimensions d . Table 1 shows some average running times of SolveNNQ and `quadprog`. When $n \geq 130$ and $n \geq 13d$, SolveNNQ is often 10 times or more faster. Figure 2 shows the plot of the natural logarithm of the average speedup of SolveNNQ over a single call of `quadprog`. For both DKSG and ZHLG and for every fixed d , the average speedup as a function of n hovers around $\Theta(n^3)$ for Ionosphere and AAL. In Appendix D.1, we show more results on Iris and HCV. Figure 3(a) shows the plot of the average $\frac{f(\mathbf{x}_{r+1}) - f(\mathbf{x}_*)}{f(\mathbf{x}_r) - f(\mathbf{x}_*)}$ against r in some of our experiments. It shows that the gap $f(\mathbf{x}_r) - f(\mathbf{x}_*)$ decreases by at least a constant factor; most of the runs show

		Ionosphere						AAL					
n	d	DKSG			ZHLG			DKSG			ZHLG		
		quadprog	ours	nnz	quadprog	ours	nnz	quadprog	ours	nnz	quadprog	ours	nnz
70	2	4.57s	1.84s	44%	2.51s	1.06s	47%	3.99s	1.72s	44%	2.36s	1.19s	52%
	4	5.78s	2.25s	47%	2.20s	0.97s	49%	4.64s	1.94s	46%	2.32s	1.27s	50%
	10	4.65s	1.55s	47%	1.86s	1.67s	59%	4.89s	1.80s	48%	1.93s	1.69s	58%
100	2	26.67s	5.41s	33%	16.31s	3.35s	36%	22.91s	5.30s	34%	15.25s	3.24s	37%
	4	43.60s	7.06s	35%	14.87s	2.77s	36%	38.63s	7.81s	37%	13.38s	2.68s	35%
	10	28.53s	5.46s	35%	13.34s	5.42s	44%	36.58s	6.00s	35%	13.34s	4.59s	43%
130	2	192.41s	11.56s	27%	144.27s	5.53s	28%	175.43s	15.81s	27%	145.83s	6.58s	28%
	4	261.54s	13.13s	27%	141.70s	6.23s	29%	221.80s	15.89s	29%	142.01s	5.88s	30%
	10	208.24s	12.02s	27%	134.95s	12.43s	36%	257.41s	14.60s	28%	135.08s	10.03s	35%
160	2	660.25s	25.39s	23%	614.71s	9.14s	24%	550.44s	26.06s	24%	613.45s	15.01s	26%
	4	888.06s	27.20s	23%	622.58s	10.74s	24%	864.51s	31.71s	24%	610.71s	14.62s	26%
	10	979.92s	22.03s	22%	598.55s	29.97s	31%	984.85s	20.86s	22%	601.50s	22.42s	30%

Table 1: Ionosphere and AAL: each data shown for a pair (n, d) is the average of the corresponding data from five runs; nnz is the percentage of the average number of non-zeros in the final solution.

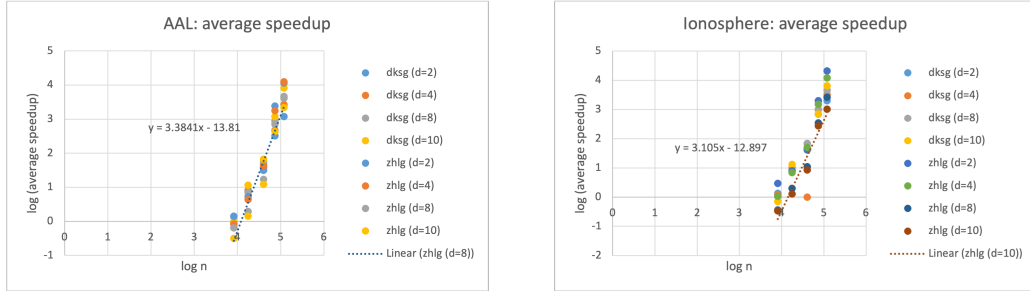


Figure 2: We plot the natural logarithm of the average speedup of SolveNNQ over a single call of quadprog for DKSG and ZHLG. The horizontal axis is $\ln n$. Data sets of different dimensions are obtained from AAL and Ionosphere.

an even faster convergence. Our lower bound in Corollary 2.1 leads to a geometric convergence if both $\frac{\|\mathbf{x}_{r+1} - \mathbf{x}_r\|}{\|\mathbf{x}_* - \mathbf{x}_r\|}$ and $\frac{\cos \angle(\mathbf{v}_r, \mathbf{x}_{r+1} - \mathbf{x}_r)}{\cos \angle(\mathbf{v}_r, \mathbf{x}_* - \mathbf{x}_r)}$ are bounded away from zero. Figure 3(b) shows the plot of the average $\frac{\|\mathbf{x}_{r+1} - \mathbf{x}_r\|}{\|\mathbf{x}_* - \mathbf{x}_r\|}$ against r . Figure 3(c) the corresponding plot of the median $\frac{\cos \angle(\mathbf{v}_r, \mathbf{x}_{r+1} - \mathbf{x}_r)}{\cos \angle(\mathbf{v}_r, \mathbf{x}_* - \mathbf{x}_r)}$ against r . The average $\frac{\|\mathbf{x}_{r+1} - \mathbf{x}_r\|}{\|\mathbf{x}_* - \mathbf{x}_r\|}$ is more than 0.4 and the median $\frac{\cos \angle(\mathbf{v}_r, \mathbf{x}_{r+1} - \mathbf{x}_r)}{\cos \angle(\mathbf{v}_r, \mathbf{x}_* - \mathbf{x}_r)}$ is more than 0.5.

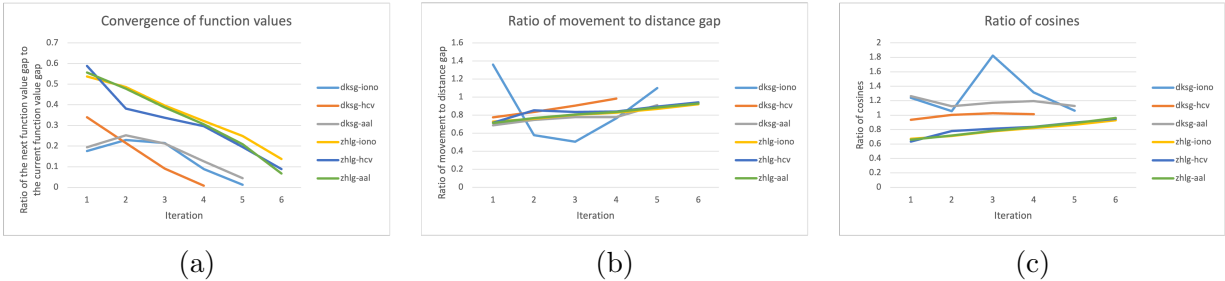
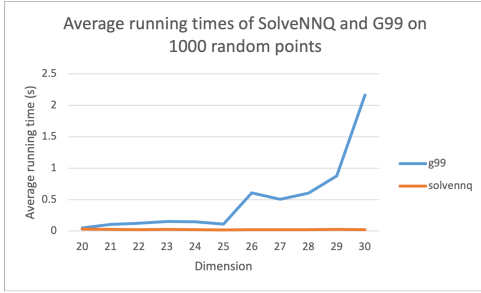


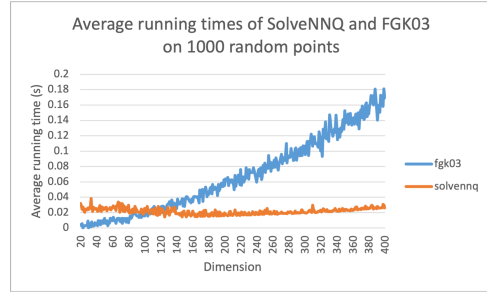
Figure 3: (a) Plot of the average $\frac{f(\mathbf{x}_{r+1}) - f(\mathbf{x}_*)}{f(\mathbf{x}_r) - f(\mathbf{x}_*)}$ against r . (b) Plot of the average $\frac{\|\mathbf{x}_{r+1} - \mathbf{x}_r\|}{\|\mathbf{x}_* - \mathbf{x}_r\|}$ against r . (c) Plot of the median $\frac{\cos \angle(\mathbf{v}_r, \mathbf{x}_{r+1} - \mathbf{x}_r)}{\cos \angle(\mathbf{v}_r, \mathbf{x}_* - \mathbf{x}_r)}$ against r .

5.2 Minimum Enclosing Ball

We experimented with two types of point sets as in previous works [21, 23, 24]. The first type is uniformly random points from a d -dimensional unit cube. The second type is nearly cospherical



(a) SolveNNQ vs G99.



(b) SolveNNQ vs FGK03.

Figure 4: Average running times on 1000 random points in a unit cube.

		MEB					
n	d	Random Points			Nearly Cospherical Points		
		quadprog	ours	nnz	quadprog	ours	nnz
1000	200	0.119s	0.026s	202	0.108s	0.339s	918
	400	0.131s	0.030s	401	0.106s	0.223s	958
	1000	0.116s	0.155s	1000	0.0931s	0.095s	1000
2000	200	0.573s	0.056s	201	0.506s	0.921s	1301
	400	0.559s	0.062s	401	0.539s	1.369s	1499
	1000	0.599s	0.161s	1001	0.554s	1.082s	1814
4000	200	3.360s	0.223s	203	2.918s	2.013s	1803
	400	3.730s	0.193s	401	2.828s	3.328s	2211
	1000	4.261s	0.304s	1001	2.862s	5.332s	2796
6000	200	10.765s	0.485s	202	9.279s	3.993s	2185
	400	11.261s	0.453s	401	8.552s	6.533s	2753
	1000	12.020s	0.546s	1001	7.934s	10.323s	3516
8000	200	20.180s	0.772s	202	19.584s	5.770s	2526
	400	24.700s	0.931s	402	19.976s	9.919s	3082
	1000	24.776s	0.918s	1001	17.719s	15.208s	3937

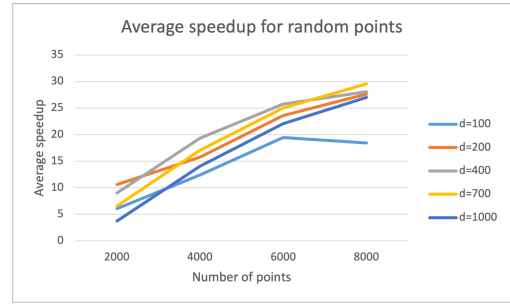


Figure 5: In the table on the left, each running time is the average over five runs, and nnz is the rounded average number of non-zeros in the final solution. The right image shows the average speedup of SolveNNQ over a single call of quadprog on random points in a unit cube.

points in \mathbb{R}^d . To generate a point set of the second type, we first draw points uniformly at random from \mathbb{S}^{d-1} . For each point \mathbf{p} drawn from \mathbb{S}^{d-1} , we pick a random number $\varepsilon \in [-10^{-4}, 10^{-4}]$ and include the point $(1 + \varepsilon)\mathbf{p}$ in the final point set. We compare SolveNNQ, quadprog, an MEB C++ code by Gärtner [22], and an MEB Java library by Fischer et al. [20]. We refer to the latter two software as G99 and FGK03, respectively. Figure 4(a) and (b) show the average running times of G99, FGK03, and SolveNNQ on 1000 random points in a unit cube as d increases. Since G99 is designed for efficiency in low dimensions, SolveNNQ is expected to outperform G99 for larger d ; this happens at $d = 20$. SolveNNQ overtakes FGK03 at 140 dimensions on random points in a unit cube. Similar trends are observed for nearly cospherical points (see Appendix D.2). In 200 dimensions or higher, SolveNNQ and a single call of quadprog outperform G99 and FGK03 on both types of point sets. The table in Figure 5 shows the results for SolveNNQ and quadprog in dimensions from 200 to 1000. When $n \geq 2000$ and $n \geq 10d$, SolveNNQ is 10 times or more faster than quadprog on random points in a unit cube; the average speedup increases roughly linearly in n for each fixed d as shown in the plot in Figure 5. For nearly cospherical point sets, the number of non-zeros in the final solution is much bigger than d , which slows down SolveNNQ significantly. Still, SolveNNQ is significantly faster than quadprog when $n \geq 6000$ and $n \geq 20d$.

5.3 Image deblurring

We experimented with four gray-scale space images *bcea*, *nph*, *sts*, and *hst* [2, 3, 7, 8]; note that the iterative scheme is efficient only when the intermediate and final solutions are sparse. We adopt the

atmospheric turbulence point spread function to generate the blurring matrix \mathbf{A} [31], which depends on a parameter σ ; the larger σ is, the blurrier the image. Multiplying \mathbf{A} with a vector representing the original image generates a vector \mathbf{b} that represents the blurred image. Working backward, we solve an NNLS problem to deblur the image: find the non-negative \mathbf{x} that minimizes $\|\mathbf{Ax} - \mathbf{b}\|^2$. We compare SolveNNQ with several software that can solve NNLS, including FISTA with backtracking (FISTABT) [5, 11], SBB [29], FNNLS [32], `lsqnonneg` of MATLAB, and a single call of `quadprog`. Figure 6 shows the results on *hst*. Table 2 shows some statistics. When the relative mean square error of an image is well below 0.01, it is visually non-distinguishable from the original. In our experiments, SolveNNQ is very efficient and it produces a very good output. More details and more results on thermal images are given in Appendix D.3. We emphasize that we do not claim a solution for image deblurring as there are many issues that we do not address; we only seek to demonstrate the potential of the iterative scheme.

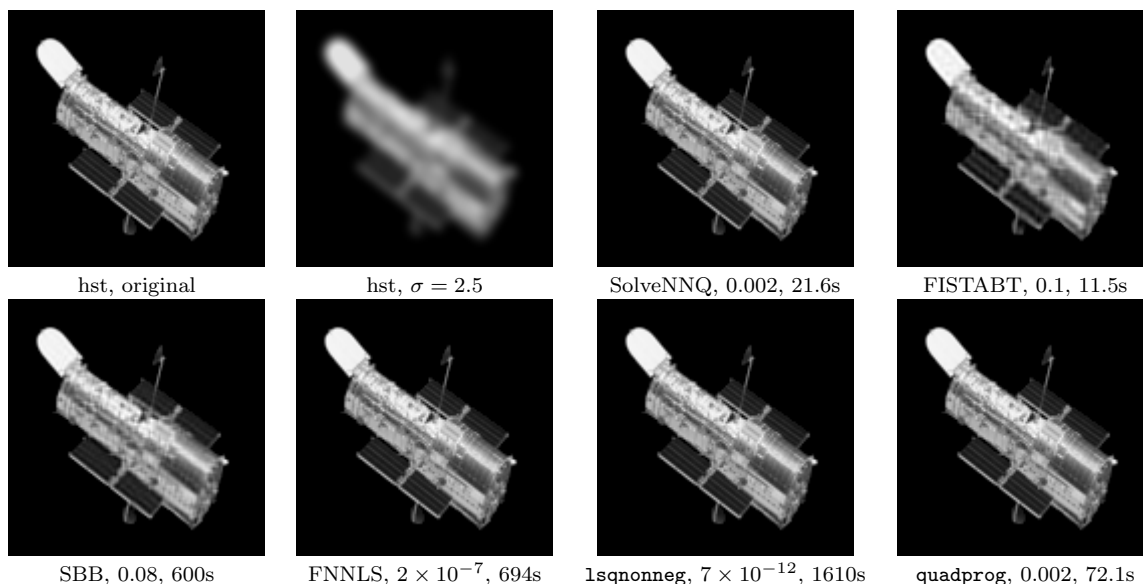


Figure 6: The upper left two images are the original and the blurred image. Under the output of each software, the first number is the relative mean square error of the intensities of the corresponding pixels between the output and the original, and the second number is the running time.

Data	σ	SolveNNQ		FISTABT		SBB		FNNLS		lsqnonneg		quadprog	
		rel. err	time	rel. err	time	rel. err	time	rel. err	time	rel. err	time	rel. err	time
bcea	1	4×10^{-5}	2.2s	0.009	1.3s	7×10^{-5}	110s	10^{-10}	33s	10^{-13}	59s	3×10^{-5}	5s
	1.5	0.001	5.1s	0.05	2.8s	0.008	600s	5×10^{-8}	137s	2×10^{-12}	267s	8×10^{-4}	11.4s
	2	0.002	9.2s	0.09	4.5s	0.02	600s	7×10^{-8}	200s	3×10^{-12}	420s	0.002	17.9s
nph	1	10^{-5}	3s	0.009	2s	3×10^{-5}	171s	7×10^{-11}	15.4s	10^{-13}	25s	3×10^{-5}	8.8s
	1.5	4×10^{-4}	5.6s	0.04	4.3s	0.009	600s	3×10^{-8}	60s	10^{-12}	105s	5×10^{-4}	17.9s
	2	7×10^{-4}	8.2s	0.06	6.8s	0.02	600s	6×10^{-8}	94s	2×10^{-12}	181s	8×10^{-4}	33.3s
sts	1	2×10^{-5}	2.1s	0.01	2.3s	4×10^{-5}	206s	8×10^{-11}	14s	9×10^{-14}	22.7s	3×10^{-5}	9.4s
	1.5	4×10^{-4}	4.9s	0.06	4.7s	0.01	600s	10^{-8}	48.9s	2×10^{-12}	87s	4×10^{-4}	20.4s
	2	5×10^{-4}	9.7s	0.1	7.1s	0.04	600s	3×10^{-8}	80s	2×10^{-12}	156s	0.001	38.6s
hst	1	2×10^{-5}	2.5s	0.02	2.3s	4×10^{-5}	275s	10^{-10}	79.4s	2×10^{-13}	182s	3×10^{-5}	9.4s
	1.5	0.001	6.5s	0.06	4.7s	0.02	600s	10^{-7}	272s	3×10^{-12}	651s	0.001	20.9s
	2	0.001	11.1s	0.1	7.4s	0.05	600s	3×10^{-7}	459s	4×10^{-12}	1060s	0.003	47.2s

Table 2: Experimental results for some space images. In the column for each software, the number on the left is the relative mean square error, and the number on the right is the running time.

References

- [1] <https://adas-dataset-v2.flirconservator.com/#downloadguide>.
- [2] https://github.com/jnagy1/IRtools/blob/master/Extra/test_data/HSTgray.jpg.
- [3] https://github.com/jnagy1/IRtools/blob/master/Extra/test_data/satellite.mat.
- [4] <https://github.com/QiaoLiuHit/LSOTB-TIR>.
- [5] <https://github.com/tiepvupsu/FISTA>.
- [6] <https://public.roboflow.com/object-detection/thermal-dogs-and-people/1>.
- [7] <https://www.skyatnightmagazine.com/advice/how-to-take-a-photo-of-the-iss/>.
- [8] <https://www.space.com/russian-progress-cargo-spacecraft-docks-space-station>.
- [9] <https://archive.ics.uci.edu/ml/datasets.php>.
- [10] N. Alon, S. Dar, M. Parnas, and D. Ron. Testing of clustering. In *Proceedings fo the 41st Annual Symposium on Foundations of Computer Science*, pages 240–250, 2000.
- [11] A. Beck and M. Teboulle. A fast iterative shrinkage-thresholding algorithm for linear inverse problems. *SIAM Journal on Imaging Sciences*, 2(1):183–202, 2009.
- [12] A. Ben-Hur, D. Horn, H.T. Siegelmann, and V. Vapnik. Support vector clustering. *Journal of Machine Learning Research*, 2:125–137, 2001.
- [13] M. Bădoiu and K.L. Clarkson. Optimal core-sets for balls. *Computational Geometry: Theory and Applications*, 40:14–22, 2008.
- [14] M. Bădoiu, S. Har-Peled, and P. Indyk. Approximate clustering via core-sets. In *Proceedings of the 34th Annual ACM Symposium on Theory of Computing*, pages 250–257, 2002.
- [15] P.H. Calamai and J.J. Moré. Projected gradient methods for linearly constrained problems. *Mathematical programming*, 39:93–116, 1987.
- [16] S.-W. Cheng, O. Cheong, T. Lee, and Z. Ren. Fitting a graph to one-dimensional data. *Theoretical Computer Science*, 867:40–49, 2021.
- [17] K.L. Clarkson. Coresets, sparse greedy approximation, and the Frank-Wolfe algorithm. *ACM Transactions on Algorithms*, 6(4), 2010.
- [18] T.F. Coleman and L.A. Hulbert. A direct active set algorithm for large sparse quadratic programs with simple bounds. *Mathematical programming*, 45:373–406, 1989.
- [19] S.I. Daitch, J.A. Kelner, and D.A. Spielman. Fitting a graph to vector data. In *Proceedings of the 26th Annual International Conference on Machine Learning*, pages 201–209, 2009.
- [20] K. Fischer, B. Gärtner, and M. Kutz. <https://github.com/hbf/miniball>.
- [21] K. Fischer, B. Gärtner, and M. Kutz. Fast smallest-enclosing-ball computation in high dimensions. In *Proceedings of the 11th Annual European Symposium on Algorithms*, pages 630–641, 2003.

- [22] B. Gärtner. <https://people.inf.ethz.ch/gaertner/subdir/software/miniball.html>.
- [23] B. Gärtner. Fast and robust smallest enclosing balls. In *Proceedings of the 7th Annual European Symposium on Algorithms*, pages 121–139, 1999.
- [24] B. Gärtner and S. Schönherr. An efficient, exact, and generic quadratic programming solver for geometric optimization. In *Proceedings of the 16th Annual Symposium on Computational Geometry*, pages 110–118, 2000.
- [25] M. Hanke, J.G. Nagy, and C. Vogel. Quasi-Newton approach to nonnegative image restorations. *Linear Algebra and Its Applications*, 316:223–236, 2000.
- [26] P.M. Hubbard. Approximating polyhedra with spheres for time-critical collision detection. *ACM Transactions on Graphics*, 15:179–210, 1996.
- [27] T. Jebara, J. Wang, and S.-F. Chang. Graph construction and b -matching for semi-supervised learning. In *Proceedings of the 26th Annual International Conference on Machine Learning*, pages 441–448, 2009.
- [28] V. Kalofolias. How to learn a graph from smooth signals. In *Proceedings of the 19th International Conference on Artificial Intelligence and Statistics*, pages 920–929, 2016.
- [29] D. Kim, S. Sra, and I.S. Dhillon. A non-monotonic method for large-scale non-negative least squares. *Optimization Methods and Software*, 28(5):1012–1039, 2013.
- [30] P. Kumar, J.S.B. Mitchell, and E.A. Yildirim. Approximate minimum enclosing balls in high dimensions using core-sets. *ACM Journal of Experimental Algorithmics*, 8, 2003.
- [31] R.L. Legendijk and J. Biemond. *Iterative Identification and Restoration of Images*. Springer, 1991.
- [32] C.L. Lawson and R.J. Hanson. *Solving least squares problems*. SIAM, 1995.
- [33] J. Matoušek, M. Sharir, and E. Welzl. A subexponential bound for linear programming. *Algorithmica*, 16:498–516, 1996.
- [34] B.L. McGlamery. Restoration of turbulence degraded images. *Journal of the Optical Society of America*, 57(3):293–297, 1967.
- [35] R.D.C. Monteiro and I. Adler. Interior path following primal-dual algorithms. Part II: convex quadratic programming. *Mathematical Programming*, 44:43–66, 1989.
- [36] K. Sekitani and Y. Yamamoto. A recursive algorithm for finding the minimum norm point in a polytope and a pair of closest points in two polytopes. *Mathematical Programming*, 61:233–249, 1993.
- [37] I.W. Tsang, J.T. Kwok, and P.-M. . Core vector machines: fast SVM training on very large data sets. *Journal of Machine Learning Research*, 6:363–392, 2005.
- [38] I.W. Tsang, J.T. Kwok, and J.M. Zurada. Generalized core vector machines. *IEEE Transactions on Neural Networks*, 17(5):1126–1140, 2006.
- [39] E. Welzl. Smallest enclosing disks (balls and ellipsoids). In *New Results and New Trends in Computer Science*, volume 555 of Lecture Notes in Computer Science, pages 359–270. Springer, 1991.

- [40] P. Wolfe. Finding the nearest point in a polytope. *Mathematical Programming*, 11:128–149, 1976.
- [41] E.A. Yildirim. Two algorithms for the minimum enclosing ball problem. *SIAM Journal on Optimization*, 19(3):1368–1391, 2008.
- [42] Y.-M. Zhang, K. Huang, X. Hou, and C.-L. Liu. Learning locality preserving graph from data. *IEEE Transactions on Cybernetics*, 44(11):2088–2098, 2014.

A Missing content in Section 2

A.1 Number of iterations when β_1 is exceeded

Let \mathbf{x}_* denote the optimal solution of the original NNQ problem.

Lemma A.1. *If β_1 is exceeded, lines 7–19 of SolveNNQ will be iterated at most $|\text{supp}(\mathbf{x}_*)|$ more times before \mathbf{x}_* is found.*

Proof. By the KKT conditions, $\nabla f(\mathbf{x}_r) = \mathbf{B}^t \mathbf{u}_r + \mathbf{C}^t \tilde{\mathbf{u}}_r + \mathbf{v}_r$, so $\langle \nabla f(\mathbf{x}_r), \mathbf{x}_* - \mathbf{x}_r \rangle = \langle \mathbf{B}^t \mathbf{u}_r, \mathbf{x}_* - \mathbf{x}_r \rangle + \langle \mathbf{C}^t \tilde{\mathbf{u}}_r, \mathbf{x}_* - \mathbf{x}_r \rangle + \langle \mathbf{v}_r, \mathbf{x}_* - \mathbf{x}_r \rangle$. By the complementary slackness, we have $\mathbf{u}_r^t (\mathbf{B} \mathbf{x}_r - \mathbf{b}) = 0$ and $\mathbf{v}_r^t \mathbf{x}_r = 0$. The former equation implies that $\mathbf{u}_r^t \mathbf{B} \mathbf{x}_r = \mathbf{u}_r^t \mathbf{b}$. By primal feasibility, $\mathbf{C} \mathbf{x}_* = \mathbf{C} \mathbf{x}_r = \mathbf{c}$ which implies that $\langle \mathbf{C}^t \tilde{\mathbf{u}}_r, \mathbf{x}_* - \mathbf{x}_r \rangle = \tilde{\mathbf{u}}_r^t (\mathbf{C} \mathbf{x}_* - \mathbf{C} \mathbf{x}_r) = 0$. As a result,

$$\langle \nabla f(\mathbf{x}_r), \mathbf{x}_* - \mathbf{x}_r \rangle = \mathbf{u}_r^t (\mathbf{B} \mathbf{x}_* - \mathbf{b}) + \mathbf{v}_r^t \mathbf{x}_*. \quad (1)$$

Primal and dual feasibilities imply that $\mathbf{B} \mathbf{x}_* \geq \mathbf{b}$ and \mathbf{u}_r have non-negative coordinates; therefore, $\mathbf{u}_r^t (\mathbf{B} \mathbf{x}_* - \mathbf{b}) \geq 0$.

We claim that $(\mathbf{v}_r)_i < 0$ for some $i \in \text{supp}(\mathbf{x}_*) \cap S_r$. Assume to the contrary that $(\mathbf{v}_r)_i \geq 0$ for all $i \in \text{supp}(\mathbf{x}_*) \cap S_r$. Then, $(\mathbf{v}_r)_i \geq 0$ for all $i \in \text{supp}(\mathbf{x}_*)$, which implies that $\mathbf{v}_r^t \mathbf{x}_* \geq 0$. Substituting $\mathbf{u}_r^t (\mathbf{B} \mathbf{x}_* - \mathbf{b}) \geq 0$ and $\mathbf{v}_r^t \mathbf{x}_* \geq 0$ into (1) gives $\langle \nabla f(\mathbf{x}_r), \mathbf{x}_* - \mathbf{x}_r \rangle \geq 0$. However, since \mathbf{x}_r is not optimal, by the convexity of f and the feasible region of the NNQ problem, $\mathbf{x}_* - \mathbf{x}_r$ is a descent direction from \mathbf{x}_r , contradicting the relation $\langle \nabla f(\mathbf{x}_r), \mathbf{x}_* - \mathbf{x}_r \rangle \geq 0$. This proves our claim.

By our claim, there must exist some index $i \in \text{supp}(\mathbf{x}_*) \cap S_r$ such that $(\mathbf{v}_r)_i < 0$. This index i must be included in E_r , which means that $i \notin S_{r+1}$ because $S_{r+1} = S_r \setminus E_r$. As a result, each iteration of lines 11 and 12 sets free at least one more element of $\text{supp}(\mathbf{x}_*)$. After at most $|\text{supp}(\mathbf{x}_*)|$ more iterations, all elements of $\text{supp}(\mathbf{x}_*)$ are free variables, which means that the solver will find \mathbf{x}_* in at most $|\text{supp}(\mathbf{x}_*)|$ more iterations. \square

A.2 Proofs of Lemma 2.1 and Corollary 2.1

We restate Lemma 2.1 and gives its proof.

Lemma 2.1 *Let $\mathbf{n} \in \mathbb{R}^{\nu}$ be any unit descent direction from \mathbf{x}_r . Let $\mathbf{y} = \mathbf{x}_r + \alpha \mathbf{n}$ for some $\alpha > 0$ be the feasible point that minimizes f on the ray from \mathbf{x}_r in direction \mathbf{n} . Then, (i) $f(\mathbf{x}_r) - f(\mathbf{y}) \leq -\|\mathbf{x}_r - \mathbf{y}\| \cdot \langle \nabla f(\mathbf{x}_r), \mathbf{n} \rangle$, and (ii) $f(\mathbf{x}_r) - f(\mathbf{y}) \geq -\frac{1}{2} \|\mathbf{x}_r - \mathbf{y}\| \cdot \langle \nabla f(\mathbf{x}_r), \mathbf{n} \rangle$.*

Proof. For all $s \in [0, 1]$, define $\mathbf{y}_s = \mathbf{x}_r + s(\mathbf{y} - \mathbf{x}_r)$. By the chain rule, we have

$$\frac{\partial f}{\partial s} = \left\langle \frac{\partial f}{\partial \mathbf{y}_s}, \frac{\partial \mathbf{y}_s}{\partial s} \right\rangle = \langle \nabla f(\mathbf{y}_s), \mathbf{y} - \mathbf{x}_r \rangle.$$

We integrate along a linear movement from \mathbf{x}_r to \mathbf{y} . Using the fact that $\nabla f(\mathbf{y}_s) = 2\mathbf{A}^t\mathbf{A}(\mathbf{x}_r + s(\mathbf{y} - \mathbf{x}_r)) + \mathbf{a} = \nabla f(\mathbf{x}_r) + 2s\mathbf{A}^t\mathbf{A}(\mathbf{y} - \mathbf{x}_r)$, we obtain

$$\begin{aligned}
f(\mathbf{y}) &= f(\mathbf{x}_r) + \int_0^1 \langle \nabla f(\mathbf{y}_s), \mathbf{y} - \mathbf{x}_r \rangle ds \\
&= f(\mathbf{x}_r) + \int_0^1 \langle \nabla f(\mathbf{x}_r), \mathbf{y} - \mathbf{x}_r \rangle ds + \int_0^1 2s \langle \mathbf{A}^t\mathbf{A}(\mathbf{y} - \mathbf{x}_r), \mathbf{y} - \mathbf{x}_r \rangle ds \\
&= f(\mathbf{x}_r) + \left[\langle \nabla f(\mathbf{x}_r), \mathbf{y} - \mathbf{x}_r \rangle \cdot s \right]_0^1 + \left[\|\mathbf{A}(\mathbf{y} - \mathbf{x}_r)\|^2 \cdot s^2 \right]_0^1 \\
&= f(\mathbf{x}_r) + \langle \nabla f(\mathbf{x}_r), \mathbf{y} - \mathbf{x}_r \rangle + \|\mathbf{A}(\mathbf{y} - \mathbf{x}_r)\|^2.
\end{aligned}$$

It follows immediately that

$$\begin{aligned}
f(\mathbf{x}_r) - f(\mathbf{y}) &= -\langle \nabla f(\mathbf{x}_r), \mathbf{y} - \mathbf{x}_r \rangle - \|\mathbf{A}(\mathbf{y} - \mathbf{x}_r)\|^2 \\
&\leq -\langle \nabla f(\mathbf{x}_r), \mathbf{y} - \mathbf{x}_r \rangle \\
&= -\|\mathbf{x}_r - \mathbf{y}\| \cdot \langle \nabla f(\mathbf{x}_r), \mathbf{n} \rangle.
\end{aligned} \tag{2}$$

This completes the proof of (i).

Consider (ii). Using $\mathbf{y}_s = \mathbf{x}_r + s(\mathbf{y} - \mathbf{x}_r) = \mathbf{y} + (1-s)(\mathbf{x}_r - \mathbf{y})$ and the fact that $\nabla f(\mathbf{y}_s) = 2\mathbf{A}^t\mathbf{A}(\mathbf{y} + (1-s)(\mathbf{x}_r - \mathbf{y})) + \mathbf{a} = \nabla f(\mathbf{y}) + 2(1-s)\mathbf{A}^t\mathbf{A}(\mathbf{x}_r - \mathbf{y})$, we carry out a symmetric derivation:

$$\begin{aligned}
f(\mathbf{x}_r) &= f(\mathbf{y}) + \int_1^0 \langle \nabla f(\mathbf{y}_s), \mathbf{y} - \mathbf{x}_r \rangle ds \\
&= f(\mathbf{y}) + \int_1^0 \langle \nabla f(\mathbf{y}), \mathbf{y} - \mathbf{x}_r \rangle ds + \int_1^0 2(1-s) \langle \mathbf{A}^t\mathbf{A}(\mathbf{x}_r - \mathbf{y}), \mathbf{y} - \mathbf{x}_r \rangle ds \\
&= f(\mathbf{y}) + \left[\langle \nabla f(\mathbf{y}), \mathbf{y} - \mathbf{x}_r \rangle \cdot s \right]_1^0 + \left[\|\mathbf{A}(\mathbf{y} - \mathbf{x}_r)\|^2 \cdot (1-s)^2 \right]_1^0 \\
&= f(\mathbf{y}) - \langle \nabla f(\mathbf{y}), \mathbf{y} - \mathbf{x}_r \rangle + \|\mathbf{A}(\mathbf{y} - \mathbf{x}_r)\|^2.
\end{aligned} \tag{3}$$

Combining (2) and (3) gives

$$f(\mathbf{x}_r) - f(\mathbf{y}) = -\frac{1}{2} \langle \nabla f(\mathbf{x}_r), \mathbf{y} - \mathbf{x}_r \rangle - \frac{1}{2} \langle \nabla f(\mathbf{y}), \mathbf{y} - \mathbf{x}_r \rangle.$$

As \mathbf{y} is the feasible point that minimizes the value of f on the ray from \mathbf{x}_r in direction \mathbf{n} , we have $\langle \nabla f(\mathbf{y}), \mathbf{y} - \mathbf{x}_r \rangle \leq 0$. Therefore,

$$f(\mathbf{x}_r) - f(\mathbf{y}) \geq -\frac{1}{2} \langle \nabla f(\mathbf{x}_r), \mathbf{y} - \mathbf{x}_r \rangle = -\frac{1}{2} \|\mathbf{x}_r - \mathbf{y}\| \cdot \langle \nabla f(\mathbf{x}_r), \mathbf{n} \rangle.$$

□

We restate Corollary 2.1 and gives its proof.

Corollary 2.1 *Let $\mathbf{n} \in \mathbb{R}^p$ be any unit descent direction from \mathbf{x}_r . Let $\mathbf{y} = \mathbf{x}_r + \alpha\mathbf{n}$ for some $\alpha > 0$ be the feasible point that minimizes f on the ray from \mathbf{x}_r in direction \mathbf{n} . Let S be an active set that is disjoint from $\text{supp}(\mathbf{x}_r) \cup \text{supp}(\mathbf{n})$. Let \mathbf{x}_{r+1} be the optimal solution for f constrained by S . Then,*

$$\frac{f(\mathbf{x}_r) - f(\mathbf{x}_{r+1})}{f(\mathbf{x}_r) - f(\mathbf{x}_*)} \geq \frac{f(\mathbf{x}_r) - f(\mathbf{y})}{f(\mathbf{x}_r) - f(\mathbf{x}_*)} \geq \frac{\|\mathbf{x}_r - \mathbf{y}\|}{2} \cdot \frac{\langle \nabla f(\mathbf{x}_r), \mathbf{n} \rangle}{\langle \nabla f(\mathbf{x}_r), \mathbf{x}_* - \mathbf{x}_r \rangle}.$$

Proof. By applying Lemma 2.1(i) to the descent direction $\mathbf{x}_* - \mathbf{x}_r$, we get $f(\mathbf{x}_r) - f(\mathbf{x}_*) \leq -\langle \nabla f(\mathbf{x}_r), \mathbf{x}_* - \mathbf{x}_r \rangle$. Since S is disjoint from $\text{supp}(\mathbf{x}_*) \cup \text{supp}(\mathbf{n})$, the feasible points on the ray from

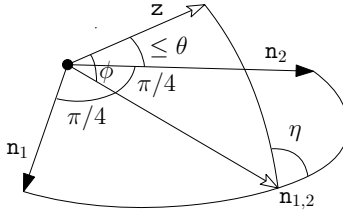


Figure 7: The vector $\mathbf{n}_{1,2}$ bisects the right angle $\angle(\mathbf{n}_1, \mathbf{n}_2)$. There are two choices for η , and we choose the angle that is at least $\pi/2$.

\mathbf{x}_r in direction \mathbf{n} are also feasible with respect to S . Therefore, $f(\mathbf{x}_r) - f(\mathbf{x}_{r+1}) \geq f(\mathbf{x}_r) - f(\mathbf{y})$. By applying Lemma 2.1(ii) to the descent direction \mathbf{n} , we get $f(\mathbf{x}_r) - f(\mathbf{x}_{r+1}) \geq f(\mathbf{x}_r) - f(\mathbf{y}) \geq -\frac{1}{2}\|\mathbf{x}_r - \mathbf{y}\| \cdot \langle \nabla f(\mathbf{x}_r), \mathbf{n} \rangle$. Dividing the lower bound for $f(\mathbf{x}_r) - f(\mathbf{x}_{r+1})$ by the upper bound for $f(\mathbf{x}_r) - f(\mathbf{x}_*)$ proves the corollary. \square

B Missing content in Section 3

B.1 Analysis for Lemma 3.1

Recall that $J_r = \text{span}(\{\mathbf{e}_i : i \in E_r\})$. The next result follows from the definitions of E_r and J_r .

Lemma B.1. *For all $i \in [\nu]$, if $i \in E_r$, then $(\mathbf{v}_r \downarrow J_r)_i = (\mathbf{v}_r)_i$; otherwise, $(\mathbf{v}_r \downarrow J_r)_i = 0$. Moreover, $-\mathbf{v}_r \downarrow J_r$ is a conical combination of $\{\mathbf{e}_i : i \in E_r\}$.*

We show that E_r gives a subset $\{\mathbf{e}_i\}$ such that $\cos \angle(\mathbf{v}_r \downarrow J_r, \mathbf{e}_i)$ is bounded away from zero.

Lemma B.2. *For any $\alpha \in (0, 1]$, there exists j in E_r with rank at most $\alpha|E_r|$ such that for every $i \in E_r$, if $i = j$ or i precedes j in E_r , then $\cos^2 \angle(\mathbf{v}_r \downarrow J_r, \mathbf{e}_i) \geq \alpha/(j \ln \nu)$.*

Proof. Consider a histogram H_1 of $\alpha/(i \ln \nu)$ against $i \in E_r$. The total length of the vertical bars in H_1 is equal to $\sum_{i \in E_r} \alpha/(i \ln \nu) \leq (\alpha/\ln \nu) \cdot \sum_{i=1}^{\nu} 1/i \leq \alpha$. Consider another histogram H_2 of $\cos^2 \angle(\mathbf{v}_r \downarrow J_r, \mathbf{e}_i)$ against $i \in E_r$. The total length of the vertical bars in H_2 is equal to $\sum_{i \in E_r} \cos^2 \angle(\mathbf{v}_r \downarrow J_r, \mathbf{e}_i)$. As $\mathbf{v}_r \downarrow J_r \in J_r$, we have $\sum_{i \in E_r} \cos^2 \angle(\mathbf{v}_r \downarrow J_r, \mathbf{e}_i) = 1$. That is, the total length of the vertical bars in H_2 is equal to 1. Recall that the indices of E_r are sorted in non-decreasing order of $(\mathbf{v}_r)_i$. As $(\mathbf{v}_r \downarrow J_r)_i = (\mathbf{v}_r)_i < 0$ for all $i \in E_r$, the ordering in E_r is the same as the non-increasing order of $\cos^2 \angle(\mathbf{v}_r \downarrow J_r, \mathbf{e}_i) = (\mathbf{v}_r \downarrow J_r)_i^2 / \|\mathbf{v}_r \downarrow J_r\|^2$. Therefore, the total length of the vertical bars in H_2 for the first $\alpha|E_r|$ indices is at least α . It implies that when we scan the indices in E_r from left to right, we must encounter an index j among the first $\alpha|E_r|$ indices such that the vertical bar in H_2 at j is not shorter than the vertical bar in H_1 at j , i.e., $\cos^2 \angle(\mathbf{v}_r \downarrow J_r, \mathbf{e}_j) \geq \alpha/(j \ln \nu)$. This index j satisfies the lemma. \square

Next, we boost the angle bound implied by Lemma B.2 by showing that $-\mathbf{v}_r \downarrow J_r$ makes a much smaller angle with some conical combination of $\{\mathbf{e}_i : i \in E_r\}$.

Lemma B.3. *Take any $c \leq 1/\sqrt{2}$. Let \mathbf{z} be a vector in \mathbb{R}^D for some $D \geq 2$. Suppose that there is a set V of unit vectors in \mathbb{R}^D such that the vectors in V are mutually orthogonal, and for every $\mathbf{n} \in V$, $\angle(\mathbf{n}, \mathbf{z}) \leq \arccos(c|V|^{-1/2})$. There exists a conical combination \mathbf{y} of the vectors in V such that $\angle(\mathbf{y}, \mathbf{z}) \leq \arccos(c/\sqrt{2})$.*

Proof. Let $\theta = \arccos(c|V|^{-1/2})$. If $\theta \leq \pi/3$, we can pick any vector $\mathbf{n} \in V$ as \mathbf{y} because $\pi/3 \leq \arccos(c/\sqrt{2})$ for $c \leq 1/\sqrt{2}$. Suppose not. Let W be a maximal subset of V whose size is a power of 2. Arbitrarily label the vectors in W as $\mathbf{n}_1, \mathbf{n}_2, \dots$. Consider the unit vector $\mathbf{n}_{1,2} = \frac{1}{\sqrt{2}}\mathbf{n}_1 + \frac{1}{\sqrt{2}}\mathbf{n}_2$. Let $\phi = \angle(\mathbf{n}_{1,2}, \mathbf{z})$. Refer to Figure 7. By assumption, $\mathbf{n}_1 \perp \mathbf{n}_2$. We choose η to be at least $\pi/2$ as explained in the caption of Figure 7. By the spherical law of cosines, $\cos \theta \leq \cos \angle(\mathbf{n}_2, \mathbf{z}) = \cos \phi \cos(\pi/4) + \sin \phi \sin(\pi/4) \cos \eta$. Note that $\cos \eta \leq 0$ as $\eta \geq \pi/2$. It implies that $\cos \phi \geq \sec(\pi/4) \cos \theta = \sqrt{2} \cos \theta$. The same analysis holds between \mathbf{z} and the unit vector $\mathbf{n}_{3,4} = \frac{1}{\sqrt{2}}\mathbf{n}_3 + \frac{1}{\sqrt{2}}\mathbf{n}_4$, and so on. In the end, we obtain $|W|/2$ vectors $\mathbf{n}_{2i-1,2i}$ for $i = 1, 2, \dots, |W|/2$ such that $\angle(\mathbf{n}_{2i-1,2i}, \mathbf{z}) \leq \arccos(\sqrt{2} \cos \theta)$. Call this the first stage. Repeat the above with the $|W|/2$ unit vectors $\mathbf{n}_{1,2}, \mathbf{n}_{3,4}, \dots$ in the second stage and so on. We end up with only one vector in $\log_2 |W|$ stages. If we ever produce a vector that makes an angle at most $\pi/3$ with \mathbf{z} before going through all $\log_2 |W|$ stages, the lemma is true. Otherwise, we produce a vector \mathbf{y} in the end such that $\cos \angle(\mathbf{y}, \mathbf{z}) \geq (\sqrt{2})^{\log_2 |W|} \cos \theta \geq (\sqrt{2})^{\log_2 |V|-1} \cos \theta \geq \sqrt{|V|/2} \cdot \cos \theta = c/\sqrt{2}$. \square

We now are ready to prove Lemma 3.1 which is restated below for convenience.

Lemma 3.1 *The vectors in $\{\mathbf{e}_i : i \text{ among the first } \tau \text{ indices in } E_r\}$ have a unit conical combination \mathbf{n}_r such that \mathbf{n}_r is a descent direction from \mathbf{x}_r and $\angle(-\mathbf{v}_r \downarrow J_r, \mathbf{n}_r) \leq \arccos(\sqrt{\alpha/(2 \ln \nu)})$, where $\alpha = \min\{1, \tau/|E_r|\}$.*

Proof. Since $-\mathbf{v}_r \downarrow J_r$ is a conical combination of $\{\mathbf{e}_i : i \in E_r\}$, $-\mathbf{v}_r \downarrow J_r$ makes a non-obtuse angle with any vector in $\{\mathbf{e}_i : i \in E_r\}$. Then, Lemmas B.2 and B.3 imply that the vectors in $\{\mathbf{e}_i : i \text{ among the first } \tau \text{ indices in } E_r\}$ have a unit conical combination \mathbf{n}_r such that $\cos \angle(-\mathbf{v}_r \downarrow J_r, \mathbf{n}_r) \geq \sqrt{\alpha/(2 \ln \nu)}$, where $\alpha = \min\{1, \tau/|E_r|\}$. For any feasible solution \mathbf{x} and any non-negative values c_1, \dots, c_ν , $\mathbf{x} + \sum_{i=1}^\nu c_i \mathbf{e}_i$ is also a feasible solution. It follows that $\mathbf{x}_r + s \mathbf{n}_r$ is a feasible solution for all $s \geq 0$. Recall that $\nabla f(\mathbf{x}_r) = \mathbf{v}_r$. Moreover, $\langle -\mathbf{v}_r \downarrow J_r, \mathbf{n}_r \rangle = \langle -\mathbf{v}_r, \mathbf{n}_r \rangle$ because $\mathbf{n}_r \in J_r$ and so the component of $-\mathbf{v}_r$ orthogonal to J_r vanishes in the inner product. Then, the acuteness of $\angle(-\mathbf{v}_r \downarrow J_r, \mathbf{n}_r)$ implies that $\langle \nabla f(\mathbf{x}_r), \mathbf{n}_r \rangle < 0$. In all, \mathbf{n}_r is a descent direction. \square

B.2 Analysis for Theorem 3.1

We restate Theorem 3.1 and give its proof.

Theorem 3.1 *Consider the application of SolveNNQ on an NNLS problem with n constraints in \mathbb{R}^d or a ZHLG problem for n points in \mathbb{R}^d . Let ν be n for NNLS or $n(n-1)/2$ for ZHLG. The initialization of SolveNNQ can be done in $T(\beta_0) + O(dn^2)$ time for NNLS or $T(\beta_0) + O(n^4)$ time for ZHLG. Suppose that the threshold β_1 on the total number of iterations is not exceeded, and there exists λ such that $\|\mathbf{x}_r - \mathbf{y}_r\| \geq \frac{1}{\lambda} \|\mathbf{x}_r - \mathbf{x}_*\|$ for all $r \geq 1$, where \mathbf{y}_r is the feasible point that minimizes f on the ray from \mathbf{x}_r in the descent direction that satisfies Lemma 3.1. Then, for all $r \geq 1$, $f(\mathbf{x}_{r+i}) - f(\mathbf{x}_*) \leq e^{-1}(f(\mathbf{x}_r) - f(\mathbf{x}_*))$ for some $i = O(\lambda \sqrt{\nu \log \nu / \tau})$, and each iteration in SolveNNQ takes $T(k + \beta_0) + O(k\nu + \beta_0^2)$ time, where $k = \max_{r \geq 1} |\text{supp}(\mathbf{x}_r)|$.*

Proof. For NNLS, \mathbf{A} is $n \times d$ and we compute $\mathbf{A}^t \mathbf{A}$ in $O(dn^2)$ time. For ZHLG, \mathbf{A} is $n(n+1)/2 \times n(n-1)/2$ and \mathbf{a} is a vector of dimension $n(n-1)/2$. Recall that $\mathbf{A}^t = \left[\frac{\mu}{2} \mathbf{U}^t \quad \frac{\ell}{2} \mathbf{I}_{n(n-1)/2} \right]$, where $\mathbf{U} \in \mathbb{R}^{n \times n(n-1)/2}$ is the incidence matrix for the complete graph. Therefore, each row of \mathbf{A}^t has at most three non-zero entries, meaning that $\mathbf{A}^t \mathbf{A}$ can be computed in $O(n^4)$ time.

The initial solution is obtained as follows. Sample β_0 indices from $[\nu]$. The initial active set

contains all indices in the range $[\nu]$ except for these sampled indices. We extract the rows and columns of $\mathbf{A}^t \mathbf{A}$ and coordinates of \mathbf{a} that correspond to these β_0 sampled indices. Then, we call the solver in $T(\beta_0)$ time to obtain the initial solution \mathbf{x}_1 .

At the beginning of every iteration, we compute $\nabla f(\mathbf{x}_r)$ and update the active set. This step can be done in $O(k\nu)$ time because \mathbf{x}_r has at most k non-zero entries. At most $k + \beta_0$ indices are absent from the updated active set because the threshold β_1 is not exceeded. We select the rows and columns of $\mathbf{A}^t \mathbf{A}$ and coordinates of \mathbf{a} that correspond to the indices absent from the active set in $O(k^2 + \beta_0^2)$ time. The subsequent call of the solver takes $T(k + \beta_0)$ time. So each iteration runs in $T(k + \beta_0) + O(k\nu + \beta_0^2)$ time. By Lemma 3.2, we need $O(\lambda\sqrt{\nu} \log \nu/\tau)$ iterations to reduce the gap $f(\mathbf{x}_r) - f(\mathbf{x}_*)$ by a factor e . \square

C Missing content in Section 4

C.1 Proofs of Lemmas 4.1 and 4.2

We restate Lemma 4.1 and give its proof.

Lemma 4.1 *Let S be an active set disjoint from $\{1\} \cup \text{supp}(\mathbf{x}_r)$. If $\langle \mathbf{v}_r \downarrow K_r, \mathbf{e}_1 \downarrow h \rangle < 0$, then $\mathbf{n}_r = \mathbf{e}_1 \downarrow h / \|\mathbf{e}_1 \downarrow h\|$ is a unit descent direction from \mathbf{x}_r with respect to S and $\cos \angle(-\mathbf{v}_r \downarrow K_r, \mathbf{n}_r) \geq \langle -\mathbf{v}_r \downarrow K_r, \mathbf{e}_1 \downarrow h \rangle \cdot \|\mathbf{v}_r \downarrow K_r\|^{-1}$.*

Proof. Since $\mathbf{n}_r = \mathbf{e}_1 \downarrow h / \|\mathbf{e}_1 \downarrow h\|$, we have $\cos \angle(-\mathbf{v}_r \downarrow K_r, \mathbf{n}_r) = \langle -\mathbf{v}_r \downarrow K_r, \mathbf{e}_1 \downarrow h \rangle \cdot \|\mathbf{v}_r \downarrow K_r\|^{-1} \cdot \|\mathbf{e}_1 \downarrow h\|^{-1}$, which is positive as $\langle \mathbf{v}_r \downarrow K_r, \mathbf{e}_1 \downarrow h \rangle < 0$ by assumption. Clearly, $\|\mathbf{e}_1 \downarrow h\| \leq 1$. Therefore, $\cos \angle(-\mathbf{v}_r \downarrow K_r, \mathbf{n}_r)$ satisfies the lemma. It remains to argue that $\mathbf{e}_1 \downarrow h$ is a descent direction with respect to the active set S . Since S is disjoint from $\{1\} \cup \text{supp}(\mathbf{x}_r)$ by the assumption of the lemma, any movement in a direction parallel to h is not obstructed by S . As we move from \mathbf{x}_r in direction $\mathbf{e}_1 \downarrow h$, our projection in \mathbf{e}_1 moves in the positive direction, and so $(\mathbf{x})_1$ increases. During the movement, for $i \notin \{1\} \cup \text{supp}(\mathbf{x}_r)$, the coordinate $(\mathbf{x})_i$ remains at zero by the definition of h . Some coordinates among $\{(\mathbf{x})_i : i \in \text{supp}(\mathbf{x}_r)\}$, which are positive, may decrease during the movement. The feasibility constraints are thus preserved for some extent of the movement. Recall from the preamble of Section 4 that $\langle \nabla f(\mathbf{x}_r), \mathbf{e}_1 \downarrow h \rangle = \langle \mathbf{v}_r, \mathbf{e}_1 \downarrow h \rangle$, which is equal to $\langle \mathbf{v}_r \downarrow K_r, \mathbf{e}_1 \downarrow h \rangle$ as $\mathbf{e}_1 \downarrow h \in K_r$. By the assumption of the lemma, $\langle \mathbf{v}_r \downarrow K_r, \mathbf{e}_1 \downarrow h \rangle < 0$. Hence, $\mathbf{e}_1 \downarrow h$ is a descent direction. \square

Next, we restate Lemma 4.2 and give its proof.

Lemma 4.2 *Suppose that there exist positive λ and γ such that $\cos \angle(-\mathbf{v}_r \downarrow K_r, \mathbf{n}_r) \geq 1/\gamma$ and $\|\mathbf{x}_r - \mathbf{y}_r\| \geq \frac{1}{\lambda} \|\mathbf{x}_r - \mathbf{x}_*\|$ for all $r \geq 1$, where \mathbf{n}_r is the unit descent direction that satisfies Lemma 4.1 with respect to the active set S_{r+1} , and \mathbf{y}_r is the feasible point that minimizes f on the ray from \mathbf{x}_r in direction \mathbf{n}_r . Then, for all $r \geq 1$, $f(\mathbf{x}_{r+i}) - f(\mathbf{x}_*) \leq e^{-1}(f(\mathbf{x}_r) - f(\mathbf{x}_*))$ for some $i \leq 2\lambda\gamma$.*

Proof. We claim that $\langle -\mathbf{v}_r, \mathbf{x}_* - \mathbf{x}_r \rangle \leq \langle -\mathbf{v}_r \downarrow K_r, \mathbf{x}_* - \mathbf{x}_r \rangle$. Note that $(-\mathbf{v}_r + \mathbf{v}_r \downarrow K_r)_i$ is equal to zero for $i \in \text{supp}(\mathbf{x}_r) \cup E_r$ and $-(\mathbf{v}_r)_i$ otherwise. By definition, for all $i \notin \text{supp}(\mathbf{x}_r) \cup E_r$, $(\mathbf{v}_r)_i \geq 0$ and so $(-\mathbf{v}_r + \mathbf{v}_r \downarrow K_r)_i = -(\mathbf{v}_r)_i \leq 0$. By the complementary slackness, if $(\mathbf{v}_r)_i > 0$, then $(\mathbf{x}_r)_i = 0$, which implies that $(\mathbf{x}_* - \mathbf{x}_r)_i \geq 0$ as \mathbf{x}_* is non-negative. Altogether, we conclude that

$$\forall i \in [\nu], (-\mathbf{v}_r + \mathbf{v}_r \downarrow K_r)_i \cdot (\mathbf{x}_* - \mathbf{x}_r)_i = \begin{cases} 0 & \text{if } i \in \text{supp}(\mathbf{x}_r) \cup E_r, \\ \leq 0 & \text{if } i \notin \text{supp}(\mathbf{x}_r) \cup E_r. \end{cases}$$

Therefore, $\langle -\mathbf{v}_r + \mathbf{v}_r \downarrow K_r, \mathbf{x}_* - \mathbf{x}_r \rangle \leq 0$, implying that $\langle -\mathbf{v}_r, \mathbf{x}_* - \mathbf{x}_r \rangle = \langle -\mathbf{v}_r \downarrow K_r, \mathbf{x}_* - \mathbf{x}_r \rangle + \langle -\mathbf{v}_r + \mathbf{v}_r \downarrow K_r, \mathbf{x}_* - \mathbf{x}_r \rangle \leq \langle -\mathbf{v}_r \downarrow K_r, \mathbf{x}_* - \mathbf{x}_r \rangle$. This proves our claim.

Recall from the preamble of Section 4 that $\langle \nabla f(\mathbf{x}_r), \mathbf{k} \rangle = \langle \mathbf{v}_r, \mathbf{k} \rangle$ for any direction \mathbf{k} that is parallel to the hyperplanes encoded by $\mathbf{M}\mathbf{x} = \mathbf{m}$. As a result, $\langle -\nabla f(\mathbf{x}_r), \mathbf{n}_r \rangle = \langle -\mathbf{v}_r, \mathbf{n}_r \rangle = \langle -\mathbf{v}_r \downarrow K_r, \mathbf{n}_r \rangle$ because $\mathbf{n}_r \in K_r$. Similarly, $\langle -\nabla f(\mathbf{x}_r), \mathbf{x}_* - \mathbf{x}_r \rangle = \langle -\mathbf{v}_r, \mathbf{x}_* - \mathbf{x}_r \rangle$, which is at most $\langle -\mathbf{v}_r \downarrow K_r, \mathbf{x}_* - \mathbf{x}_r \rangle$ by the claim that we proved earlier.

We apply Corollary 2.1 and the assumptions of $\cos \angle(-\mathbf{v}_r \downarrow K_r, \mathbf{n}_r) \geq 1/\gamma$ and $\|\mathbf{x}_r - \mathbf{y}_r\| \geq \frac{1}{\lambda} \|\mathbf{x}_r - \mathbf{x}_*\|$. Hence,

$$\frac{f(\mathbf{x}_r) - f(\mathbf{x}_{r+1})}{f(\mathbf{x}_r) - f(\mathbf{x}_*)} \geq \frac{\|\mathbf{x}_r - \mathbf{y}_r\| \cdot \langle -\mathbf{v}_r \downarrow K_r, \mathbf{n}_r \rangle}{2 \langle -\mathbf{v}_r \downarrow K_r, \mathbf{x}_* - \mathbf{x}_r \rangle} \geq \frac{\|\mathbf{x}_r - \mathbf{y}_r\|}{\|\mathbf{x}_r - \mathbf{x}_*\|} \cdot \frac{1}{2\gamma} \geq \frac{1}{2\lambda\gamma}.$$

It follows that $f(\mathbf{x}_{r+1}) - f(\mathbf{x}_*) \leq \left(1 - \frac{1}{2\lambda\gamma}\right) \cdot (f(\mathbf{x}_r) - f(\mathbf{x}_*))$. As a result, in at most $2\lambda\gamma$ iterations,

$$f(\mathbf{x}_{r+2\lambda\gamma}) - f(\mathbf{x}_*) \leq \left(1 - \frac{1}{2\lambda\gamma}\right)^{2\lambda\gamma} \cdot (f(\mathbf{x}_r) - f(\mathbf{x}_*)) \leq e^{-1} \cdot (f(\mathbf{x}_r) - f(\mathbf{x}_*)).$$

□

C.2 Convergence analysis for DKSG

We add one slack variable per constraint in $\mathbf{B}\mathbf{x} \geq \mathbf{1}_n$. This gives n slack variables and a total of $n(n+1)/2$ variables. That is, the ambient space expands to $\mathbb{R}^{n(n+1)/2}$.

For every $\hat{\mathbf{x}} \in \mathbb{R}^{n(n+1)/2}$, the slack variables are represented by the last n coordinates of $\hat{\mathbf{x}}$. The constraint matrix becomes $\hat{\mathbf{B}} = [\mathbf{B} \quad -\mathbf{I}_n]$ and the feasibility constraints become $\hat{\mathbf{B}}\hat{\mathbf{x}} = \mathbf{1}_{n(n+1)/2}$. Similarly, we expand the matrix \mathbf{A} to $\hat{\mathbf{A}} = [\mathbf{A} \quad \mathbf{0}_{n,n}]$, where $\mathbf{0}_{n,n}$ denotes the $n \times n$ zero matrix. Let $\hat{f} : \mathbb{R}^{n(n+1)/2} \rightarrow \mathbb{R}$ denote the corresponding objective function.

The dual variables \mathbf{u} for the constraints $\mathbf{B}\mathbf{x} \geq \mathbf{1}_n$ are still the dual variables for $\hat{\mathbf{B}}\hat{\mathbf{x}} = \mathbf{1}_n$. We have a new set of dual variables $\hat{\mathbf{v}} \geq \mathbf{0}_{n(n+1)/2}$ for the primal variables $\hat{\mathbf{x}}$. One can verify that if $(\mathbf{u}, \mathbf{v}, \mathbf{x})$ is an optimal solution for the original system, then $(\mathbf{u}, \hat{\mathbf{v}}, \hat{\mathbf{x}})$ with the following setting satisfies the KKT conditions for the extended system, i.e., it is an optimal solution for the extended system:

- For all $j \in [n(n-1)/2]$, $(\hat{\mathbf{x}})_j = (\mathbf{x})_j$.
- For all $j \in [n(n-1)/2 + 1, n(n+1)/2]$, $(\hat{\mathbf{x}})_j = (\mathbf{B})_{a,*} \cdot \mathbf{x} - 1$, where $a = j - n(n-1)/2$ and $(\mathbf{B})_{a,*}$ denotes the a -th row of \mathbf{B} .
- For all $j \in [n(n-1)/2]$, $(\hat{\mathbf{v}})_j = (\mathbf{v})_j$.
- For all $j \in [n(n-1)/2 + 1, n(n+1)/2]$, $(\hat{\mathbf{v}})_j = (\mathbf{u})_a$, where $a = j - n(n-1)/2$.

Conversely, if $(\mathbf{u}, \hat{\mathbf{v}}, \hat{\mathbf{x}})$ is an optimal solution for the extended system, we verify that $(\mathbf{u}, \mathbf{v}, \mathbf{x})$ satisfies the KKT conditions for the original system, i.e., $(\mathbf{u}, \mathbf{v}, \mathbf{x})$ is an optimal solution of the original system. By the KKT conditions on the extended system, we have $\hat{\mathbf{x}} \geq \mathbf{0}_{n(n+1)/2}$, $\hat{\mathbf{v}} \geq \mathbf{0}_{n(n+1)/2}$, and

$$\begin{bmatrix} \nabla f(\mathbf{x}) \\ \mathbf{0}_n \end{bmatrix} - \hat{\mathbf{B}}^t \mathbf{u} - \hat{\mathbf{v}} = \mathbf{0}_{n(n+1)/2} \Rightarrow \hat{\mathbf{v}} = \begin{bmatrix} \nabla f(\mathbf{x}) - \mathbf{B}^t \mathbf{u} \\ \mathbf{u} \end{bmatrix}.$$

The fact that $\hat{\mathbf{v}} \geq \mathbf{0}_{n(n+1)/2}$ implies that $\mathbf{u} \geq \mathbf{0}_n$. By our setting, \mathbf{x} and \mathbf{v} consist of the first $n(n-1)/2$ coordinates of $\hat{\mathbf{x}}$ and $\hat{\mathbf{v}}$, respectively; therefore, $\mathbf{v} = \nabla f(\mathbf{x}) - \mathbf{B}^t \mathbf{u}$, $\mathbf{v} \geq \mathbf{0}_{n(n-1)/2}$, and

$\mathbf{x} \geq 0_{n(n-1)/2}$. The non-negative slack variables ensure that $\mathbf{B}\mathbf{x} \geq \mathbf{1}_n$. The complementary slackness on the extended system guarantees that $(\mathbf{v})_i \cdot (\mathbf{x})_i = (\hat{\mathbf{v}})_i \cdot (\hat{\mathbf{x}})_i = 0$ for $i \in [n(n-1)/2]$. We show that $(\mathbf{u})_a \cdot ((\mathbf{B})_{a,*}\mathbf{x} - \mathbf{1}) = 0$ for $a \in [n]$. For all $a \in [n]$, if $(\mathbf{B})_{a,*}\mathbf{x} > \mathbf{1}$, the a -th slack variable is positive which forces $(\mathbf{u})_a = (\hat{\mathbf{v}})_{n(n-1)/2+a} = 0$ by the complementary slackness on the extended system. In the reverse direction, if $(\mathbf{u})_a = (\hat{\mathbf{v}})_{n(n-1)/2+a} > 0$, the a -th slack variable is zero by the complementary slackness on the extended system; this forces $(\mathbf{B})_{a,*}\mathbf{x} = \mathbf{1}$. We complete the analysis that $(\mathbf{u}, \mathbf{v}, \mathbf{x})$ satisfies the KKT conditions for the original system.

In the case that some primal variables belong to the active set, we allow the corresponding $(\hat{\mathbf{v}})_i$ to be unrestricted. The slack variables are always free because SolveNNQ is unaware of them.

Let $(\mathbf{u}_r, \hat{\mathbf{v}}_r, \hat{\mathbf{x}}_r)$ be the extended solution corresponding to $(\mathbf{u}_r, \mathbf{v}_r, \mathbf{x}_r)$.

We assume that $(\mathbf{v}_r)_1 = \min_{i \in E_r} (\mathbf{v}_r)_i$ and that the edge with index 1 is $\mathbf{p}_1\mathbf{p}_2$. For DKSG, the instantiation of the definition of I_a for DKSG is as follows:

$$\forall a \in [n], I_a = \text{intersection of } \text{supp}(\hat{\mathbf{x}}_r) \text{ and the set } \{n(n-1)/2 + a\} \cup \{i : i \text{ is the index of a complete graph edge incident to } \mathbf{p}_a\}.$$

Note that $1 \notin I_a$ for $a \in [n]$. The set I_a is not empty because every node must be incident to some edge in the graph induced by $\hat{\mathbf{x}}_r$ in order that the incident edges of that node have a total weight of at least 1. There may be some slack variables in $\text{supp}(\hat{\mathbf{x}}_r)$, but E_r does not contain any slack variable.

Correspondingly, the instantiations of the definitions of H_a for $a \in [n]$ and the affine subspace h are as follows:

$$\forall a \in [n], H_a = \left\{ \hat{\mathbf{x}} \in \mathbb{R}^{n(n+1)/2} : \sum_{i \in \{1\} \cup I_a} (\hat{\mathbf{B}})_{a,i} \cdot (\mathbf{x})_i = 1 \wedge \forall i \notin \{1\} \cup \text{supp}(\hat{\mathbf{x}}_r), (\hat{\mathbf{x}})_i = 0 \right\},$$

$$h = \bigcap_{a \in [n]} H_a.$$

Regarding the vector \mathbf{k}_a that is normal to H_a for $a \in [n]$, note that $(\mathbf{k}_a)_1 = 0$ if $a \notin \{1, 2\}$. As a result,

$$\mathbf{e}_1 \downarrow h = \mathbf{e}_1 - \sum_{a \in [n]} \langle \mathbf{e}_1, \mathbf{k}_a \rangle \mathbf{k}_a = \mathbf{e}_1 - \sum_{a=1}^2 \langle \mathbf{e}_1, \mathbf{k}_a \rangle \mathbf{k}_a.$$

For every $a \in \{1, 2\}$ and every $i \in \{1\} \cup I_a$, if $i \in [n(n-1)/2]$, then $(\hat{\mathbf{B}})_{a,i} = 1$; otherwise, i must be equal to $n(n-1)/2 + a$ which means that $(\hat{\mathbf{B}})_{a,i} = -1$. Therefore,

$$\forall a \in \{1, 2\}, \forall i \in [n(n+1)/2], \frac{(\hat{\mathbf{B}})_{a,i}^2}{\sum_{j \in \{1\} \cup I_a} (\hat{\mathbf{B}})_{a,j}^2} = \frac{(\hat{\mathbf{B}})_{a,i}^2}{|I_a| + 1}.$$

Recall that the normal vector \mathbf{k}_a is defined as:

$$\forall a \in \{1, 2\}, \forall i \in [n(n+1)/2], (\mathbf{k}_a)_i = \begin{cases} \frac{(\hat{\mathbf{B}})_{a,i}}{\sqrt{\sum_{j \in \{1\} \cup I_a} (\hat{\mathbf{B}})_{a,j}^2}} & \text{if } i \in \{1\} \cup I_a, \\ 0 & \text{otherwise.} \end{cases}$$

It follows that:

$$\forall a \in \{1, 2\}, \forall i \in [n(n+1)/2], \quad (\mathbf{k}_a)_i = \begin{cases} \frac{1}{\sqrt{|I_a|+1}} & \text{if } i = 1, \\ \frac{1}{\sqrt{|I_a|+1}} & \text{if } i \in [n(n-1)/2] \text{ and } i \in I_a, \\ -\frac{1}{\sqrt{|I_a|+1}} & \text{if } i = n(n-1)/2 + a \text{ and } i \in I_a, \\ 0 & \text{otherwise.} \end{cases}$$

Therefore,

$$\mathbf{e}_1 \downarrow h = \mathbf{e}_1 - \sum_{a=1}^2 \frac{\mathbf{k}_a}{\sqrt{|I_a|+1}}.$$

Taking the inner product with $\hat{\mathbf{v}}_r \downarrow K_r$ results in:

$$\begin{aligned} \langle \hat{\mathbf{v}}_r \downarrow K_r, \mathbf{e}_1 \downarrow h \rangle &= \langle \hat{\mathbf{v}}_r \downarrow K_r, \mathbf{e}_1 \rangle - \sum_{a=1}^2 \frac{\langle \hat{\mathbf{v}}_r \downarrow K_r, \mathbf{k}_a \rangle}{\sqrt{|I_a|+1}} \\ &= (\hat{\mathbf{v}}_r)_1 - \sum_{a=1}^2 \frac{\langle \hat{\mathbf{v}}_r \downarrow K_r, \mathbf{k}_a \rangle}{\sqrt{|I_a|+1}}. \end{aligned}$$

The inner product $\langle \hat{\mathbf{v}}_r \downarrow K_r, \mathbf{k}_a \rangle$ can be written as:

$$\langle \hat{\mathbf{v}}_r \downarrow K_r, \mathbf{k}_a \rangle = \frac{(\hat{\mathbf{v}}_r)_1}{\sqrt{|I_a|+1}} + \sum_{i \in [n(n-1)/2] \cap I_a} \frac{(\hat{\mathbf{v}}_r)_i}{\sqrt{|I_a|+1}} - \frac{\delta_a \cdot (\mathbf{u}_r)_a}{\sqrt{|I_a|+1}}, \quad (4)$$

where $\delta_a = 1$ if $n(n-1)/2 + a \in \text{supp}(\hat{\mathbf{x}}_r)$, and $\delta_a = 0$ otherwise. This setting of δ_a arises from the fact that for $i > n(n-1)/2$, if $i = n(n-1)/2 + a \in \text{supp}(\hat{\mathbf{x}}_r)$, then $(\mathbf{v}_r \downarrow K_r)_i = (\hat{\mathbf{v}}_r)_i = (\mathbf{u}_r)_a$; otherwise, $(\mathbf{v}_r \downarrow K_r)_i = 0$. If $i \in [n(n-1)/2] \cap I_a$, then $i \in \text{supp}(\mathbf{x}_r)$, which implies that $(\hat{\mathbf{v}}_r)_i = (\mathbf{v}_r)_i = 0$. So the middle term in (4) is zero. If $\delta_a = 1$, the presence of the a -th slack variable in $\text{supp}(\hat{\mathbf{x}}_r)$ means that the a -th constraint in $\mathbf{B}\mathbf{x} \geq \mathbf{1}_n$ is not tight, implying that $(\mathbf{u}_r)_a = 0$ by the complementary slackness. We conclude that

$$\langle \hat{\mathbf{v}}_r \downarrow K_r, \mathbf{e}_1 \downarrow h \rangle = (\mathbf{v}_r)_1 - \sum_{a=1}^2 \frac{(\mathbf{v}_r)_1}{|I_a|+1}. \quad (5)$$

To invoke Lemma 4.1, we need to show that $\langle \hat{\mathbf{v}}_r \downarrow K_r, \mathbf{e}_1 \downarrow h \rangle < 0$. The technical hurdle is that both $|I_1|$ and $|I_2|$ may be equal to 1 in which case the right hand side of (5) becomes zero. That is, both \mathbf{p}_1 and \mathbf{p}_2 are incident to exactly one edge with weight 1 in the graph induced by $\hat{\mathbf{x}}_r$. This is a degenerate situation in some sense. We perturb the problem as follows so that $|I_1| \geq 2$. We add a dummy point \mathbf{p}_{n+1} arbitrarily close to \mathbf{p}_1 and insert the edge $\mathbf{p}_1\mathbf{p}_{n+1}$. We add a new constraint that forces the weight of $\mathbf{p}_1\mathbf{p}_{n+1}$ to be an arbitrarily small positive value ε . At the same time, we need to allow the sums of edge weights incident to \mathbf{p}_1 to be bounded by $1 + \varepsilon$ from below instead of 1. We do not allow \mathbf{p}_{n+1} to be connected to any point among $\mathbf{p}_2, \dots, \mathbf{p}_n$. The effect is that we force \mathbf{p}_1 to be incident to at least two edges in the graph induced by the current solution. There

is at least one edge that connects \mathbf{p}_1 to another point among $\mathbf{p}_2, \dots, \mathbf{p}_n$ because the sum of edge weights between these points and \mathbf{p}_i has to be at least 1. There is now also the edge $\mathbf{p}_1\mathbf{p}_{n+1}$, thus making $|I_1| \geq 2$. In the linear algebraic formulation, it means that the ambient space expands to $\mathbb{R}^{n(n+1)/2+1}$, $\hat{\mathbf{x}}_r$ gains a last coordinate $(\hat{\mathbf{x}}_r)_{n(n+1)/2+1}$ that represents the weight ε of $\mathbf{p}_1\mathbf{p}_{n+1}$. The vector $\hat{\mathbf{v}}_r$ also gains a corresponding coordinate. There is also a new constraint: $(\hat{\mathbf{x}})_{n(n+1)/2+1} = \varepsilon$. The new index $n(n+1)/2+1$ belongs to $\text{supp}(\hat{\mathbf{x}}_r)$ because $(\hat{\mathbf{x}}_r)_{n(n+1)/2+1}$ is forced to be $\varepsilon > 0$. As a result, $(\hat{\mathbf{v}}_r)_{n(n+1)/2+1}$ must be zero due to complementary slackness. We emphasize that SolveNNQ is oblivious of this dummy point \mathbf{p}_{n+1} and the problem perturbation associated with it; the problem perturbation is introduced for the sake of analysis only. Given a solution $\hat{\mathbf{x}}_r \in \mathbb{R}^{n(n+1)/2+1}$ that satisfies the KKT conditions with respect to the extended system with the addition of \mathbf{p}_{n+1} , one can simply remove the last coordinate to obtain a solution $\hat{\mathbf{x}}_r \in \mathbb{R}^{n(n+1)/2}$ for the original extended system without \mathbf{p}_{n+1} that satisfies the KKT conditions too. The addition of $\mathbf{p}_1\mathbf{p}_{n+1}$ increases the dimension of K_r by one, but since $(\hat{\mathbf{v}}_r)_{n(n+1)/2+1} = 0$, the projection $\hat{\mathbf{v}}_r \downarrow K_r$ remains unchanged by the increase in the dimension of K_r . After adding $\mathbf{p}_1\mathbf{p}_{n+1}$, the affine subspace h is merely translated. Therefore, there is no effect on the inner product $\langle \hat{\mathbf{v}}_r \downarrow K_r, \mathbf{e}_1 \downarrow h \rangle$ by adding \mathbf{p}_{n+1} . Hence, we will abuse the notation slightly by not changing the notation, staying in $\mathbb{R}^{n(n+1)/2}$ instead of $\mathbb{R}^{n(n+1)/2+1}$, and asserting that $|I_1| \geq 2$. We conclude that:

$$\langle \hat{\mathbf{v}}_r \downarrow K_r, \mathbf{e}_1 \downarrow h \rangle = (\mathbf{v}_r)_1 - \sum_{a=1}^2 \frac{(\mathbf{v}_r)_1}{|I_a| + 1} \leq (\mathbf{v}_r)_1 - \left(\frac{1}{3} + \frac{1}{2} \right) (\mathbf{v}_r)_1 = \frac{1}{6} (\mathbf{v}_r)_1 < 0.$$

A side effect is that the dimension of h is positive; otherwise, $\mathbf{e}_1 \downarrow h$ would be the zero vector, rendering the inner product $\langle \hat{\mathbf{v}}_r \downarrow K_r, \mathbf{e}_1 \downarrow h \rangle$ zero, a contradiction.

We are almost ready to invoke Lemma 4.1 except for an upper bound of $\|\hat{\mathbf{v}}_r \downarrow K_r\|$. We have $\|\hat{\mathbf{v}}_r \downarrow K_r\|^2 = \sum_{i \in E_r} (\mathbf{v}_r)_i^2 + \sum_{a=1}^n \delta_a \cdot (\mathbf{u}_r)_a^2$, where $\delta_a = 1$ if $n(n-1)/2 + a \in \text{supp}(\hat{\mathbf{x}}_r)$, and $\delta_a = 0$ otherwise. We have argued previously that $(\mathbf{u}_r)_a = 0$ if $\delta_a = 1$. As a result,

$$\|\hat{\mathbf{v}}_r \downarrow K_r\| = \sqrt{\sum_{i \in E_r} (\mathbf{v}_r)_i^2} \leq \sqrt{|E_r|} \cdot (-\mathbf{v}_r)_1.$$

By Lemma 4.1, $\cos \angle(-\hat{\mathbf{v}}_r \downarrow K_r, \mathbf{e}_1 \downarrow h) \geq -\frac{1}{6} (\mathbf{v}_r)_1 \cdot (\sqrt{|E_r|} \cdot (-\mathbf{v}_r)_1)^{-1} = \frac{1}{6\sqrt{|E_r|}} \geq \frac{1}{6} \cdot \sqrt{\frac{2}{n(n-1)}}$. Substituting this result into Lemma 4.2 shows that SolveNNQ reduces $f(\mathbf{x}_r) - f(\mathbf{x}_*)$ by a factor e in $O(\lambda n)$ iterations.

C.3 Proof of Theorem 4.1

We restate Theorem 4.1 and give its proof.

Theorem 4.1 *Consider running SolveNNQ on an MEB, PD, or DKSG problem. Let $k = \max_{r \geq 1} |\text{supp}(\mathbf{x}_r)|$. For all $r \geq 1$, there is a unit descent direction \mathbf{n}_r from \mathbf{x}_r that satisfies Lemma 4.1 so that $\cos \angle(-\mathbf{v}_r \downarrow K_r, \mathbf{n}_r) \geq 1/\gamma$, where γ is $\Theta(\sqrt{n})$ for MEB, $\Theta(\sqrt{m+n})$ for PD, and $\Theta(n)$ for DKSG. Suppose that the threshold β_1 on the number of iterations is not exceeded, and that $\|\mathbf{x}_r - \mathbf{y}_r\| \geq \frac{1}{\lambda} \|\mathbf{x}_r - \mathbf{x}_*\|$ for all $r \geq 1$, where \mathbf{y}_r is the feasible point that minimizes f on the ray from \mathbf{x}_r in direction \mathbf{n}_r .*

- MEB: Initialization takes $T(d+1) + O(dn^2)$ time. For $r \geq 1$, $f(\mathbf{x}_{r+i}) - f(\mathbf{x}_*) \leq e^{-1}(f(\mathbf{x}_r) - f(\mathbf{x}_*))$ for some $i = O(\lambda\sqrt{n})$. Each iteration takes $T(k + \beta_0) + O(kn + \beta_0^2)$ time.
- PD: Initialization takes $O(dm^2 + dn^2)$ time. For $r \geq 1$, $f(\mathbf{x}_{r+i}) - f(\mathbf{x}_*) \leq e^{-1}(f(\mathbf{x}_r) - f(\mathbf{x}_*))$ for some $i = O(\lambda\sqrt{m+n})$. Each iteration takes $T(k + \beta_0) + O(km + kn + \beta_0^2)$ time.

- DKSG: Initialization takes $T(n + \beta_0 - 1) + O(dn^4 + \beta_0^2)$ time. For $r \geq 1$, $f(\mathbf{x}_{r+i}) - f(\mathbf{x}_*) \leq e^{-1}(f(\mathbf{x}_r) - f(\mathbf{x}_*))$ for some $i = O(\lambda n)$. Each iteration takes $T(k + \beta_0) + O(kn^2 + \beta_0^2)$ time.

Proof. Consider MEB. Recall that $\mathbf{A} = [\mathbf{p}_1 \dots \mathbf{p}_n]$ and $\mathbf{a} = [\|\mathbf{p}_1\|^2 \dots \|\mathbf{p}_n\|^2]$. We compute $\mathbf{A}^t \mathbf{A}$ and \mathbf{a} in $O(dn^2)$ time. We compute the point $\frac{1}{n} \sum_{i=1}^n \mathbf{p}_i$ and find the $d + 1$ farthest input points from it. We set up the initial active set to contain all indices in $[n]$ except for the indices of these $d + 1$ farthest points. We extract in $O(d^2)$ time the rows and columns of $\mathbf{A}^t \mathbf{A}$ and coordinates of \mathbf{a} that correspond to the indices of those $d + 1$ farthest points. We then call the solver in $T(d + 1)$ time to obtain the initial solution $(\tilde{\mathbf{u}}_1, \mathbf{x}_1)$. In each iteration afterwards, we compute $\nabla f(\mathbf{x}_r) - \mathbf{1}_n^t \tilde{\mathbf{u}}_r$ and update the active set, which can be done in $O(kn)$ time because \mathbf{x}_r has at most k non-zero entries. Since the threshold β_1 is not exceeded, we select at most β_0 new variables to be freed. We extract in $O(k^2 + \beta_0^2)$ time the rows and columns of $\mathbf{A}^t \mathbf{A}$ and coordinates of \mathbf{a} that correspond to the indices absent from the updated active set. Then, we call the solver in $T(k + \beta_0)$ time. So each iteration takes $T(k + \beta_0) + O(kn + \beta_0^2)$ time. By Lemma 4.2 with $\gamma = \Theta(\sqrt{n})$, it takes $O(\lambda\sqrt{n})$ iterations to reduce $f(\mathbf{x}_r) - f(\mathbf{x}_*)$ by a factor e .

The analysis for PD is similar. The matrix \mathbf{A} is $[\mathbf{p}_1, \dots, \mathbf{p}_m, -\mathbf{q}_1, \dots, -\mathbf{q}_n]$ (see Appendix D.4). We first compute $\mathbf{A}^t \mathbf{A}$ in $O(dm^2 + dn^2)$ time. We pick six arbitrary points, three among $\mathbf{p}_1, \dots, \mathbf{p}_m$ and three among $\mathbf{q}_1, \dots, \mathbf{q}_n$. The initial active set includes all indices in $[m + n]$ except those of these six selected points. Then, we call the solver in $T(6, 2) = O(1)$ time to get the initial solution $(\tilde{\mathbf{u}}_1, \mathbf{x}_1)$. In each iteration afterwards, we compute $\nabla f(\mathbf{x}_r) - \mathbf{C}^t \tilde{\mathbf{u}}_r$ and update the active set, which can be done in $O(km + kn)$ time because \mathbf{x}_r has at most k non-zero entries. Since the threshold β_1 is not exceeded, we select at most β_0 new variables to be freed. We extract in $O(k^2 + \beta_0^2)$ time the rows and columns of $\mathbf{A}^t \mathbf{A}$ that correspond to the indices absent from the updated active set. Then, we call the solver in $T(k + \beta_0)$ time. So each iteration takes $T(k + \beta_0) + O(km + kn + \beta_0^2)$ time. By Lemma 4.2 with $\gamma = \Theta(\sqrt{m + n})$, it takes $O(\lambda\sqrt{m + n})$ iterations to reduce $f(\mathbf{x}_r) - f(\mathbf{x}_*)$ by a factor e .

Consider DKSG, We first compute $\mathbf{A}^t \mathbf{A}$. Recall that \mathbf{A} is $dn \times n(n - 1)/2$, and \mathbf{A} resembles the incidence matrix for the complete graph in the sense that every non-zero entry of the incidence matrix gives rise to d non-zero entries in the same column in \mathbf{A} . There are at most two non-zero entries in each column of the incidence matrix. Therefore, computing $\mathbf{A}^t \mathbf{A}$ takes $O(dn^4)$ time. We form an initial graph as follows. Randomly include β_0 edges by sampling indices from $[n(n - 1)/2]$. Also, pick a node and connect it to all other $n - 1$ nodes in order to guarantee that the initial graph admits a feasible solution for the DKSG problem. There are at most $n + \beta_0 - 1$ edges. The initial active set contains all indices in the range $[n(n - 1)/2]$ except for the indices of the edges of the initial graph. We extract in $O(n^2 + \beta_0^2)$ time the rows and columns of $\mathbf{A}^t \mathbf{A}$ that correspond to the edges of the initial graph. Then, we call the solver in $T(n + \beta_0 - 1)$ time to obtain the initial solution $(\mathbf{u}_1, \mathbf{x}_1)$. At the beginning of every iteration, we compute $\nabla f(\mathbf{x}_r)$ and update the active set. This can be done in $O(kn^2)$ time because \mathbf{x}_r has at most k non-zero entries. Since the threshold β_1 is not exceeded, at most $k + \beta_0$ indices are absent from the updated active set. We extract the corresponding rows and columns of $\mathbf{A}^t \mathbf{A}$ in $O(k^2 + \beta_0^2)$ time. The subsequent call of the solver takes $T(k + \beta_0)$ time. So each iteration runs in $T(k + \beta_0) + O(kn^2 + \beta_0^2)$ time. By Lemma 4.2 with $\gamma = \Theta(n)$, we need $O(\lambda n)$ iterations to reduce $f(\mathbf{x}_r) - f(\mathbf{x}_*)$ by a factor e . \square

D More experimental results

D.1 More results on DKSG and ZHLG

Table 3 shows some average running times of SolveNNQ and quadprog on Iris and HCV. When $n \geq 130$ and $n \geq 13d$, SolveNNQ is often 10 times or more faster than a single call of quadprog. Figure 8 shows the plot of the natural logarithm of the average speedup of SolveNNQ over a single call of quadprog against $\ln n$ for different dimension d . For both DKSG and ZHLG and for every fixed d , the average speedup as a function of n is $\Omega(n^{2.7})$.

IRIS							
n	d	DKSG			ZHLG		
		quadprog	ours	nnz	quadprog	ours	nnz
70	2	5.61s	2.00s	43%	2.76s	1.21s	47%
	3	5.66s	2.09s	44%	2.61s	1.15s	48%
	4	4.88s	2.10s	45%	2.23s	1.18s	50%
100	2	43.87s	6.55s	33%	17.63s	2.13s	34%
	3	37.56s	5.92s	33%	15.92s	2.64s	36%
	4	42.69s	5.95s	33%	15.24s	2.95s	37%
130	2	241.59s	13.29s	26%	148.34s	5.62s	29%
	3	199.22s	12.20s	27%	150.54s	5.34s	28%
	4	256.28s	13.96s	27%	151.87s	6.20s	30%
150	2	504.21s	20.15s	23%	414.79s	8.38s	25%
	3	510.55s	19.81s	24%	398.06s	7.80s	26%
	4	565.89s	21.04s	24%	390.47s	7.36s	26%

HCV							
n	d	DKSG			ZHLG		
		quadprog	ours	nnz	quadprog	ours	nnz
70	2	3.68s	1.16s	43%	2.65s	0.84s	45%
	4	5.22s	1.71s	44%	2.13s	0.88s	45%
	10	4.55s	1.35s	43%	1.88s	2.06s	62%
100	2	13.02s	3.50s	32%	15.20s	2.00s	32%
	4	39.50s	4.84s	33%	13.03s	2.35s	32%
	10	29.79s	3.65s	31%	12.78s	8.32s	48%
130	2	108.10s	6.90s	28%	141.20s	3.07s	24%
	4	180.42s	12.05s	27%	138.05s	3.78s	24%
	10	184.51s	8.16s	24%	133.91s	21.17s	38%
160	2	551.43s	17.32s	24%	613.29s	5.22s	20%
	4	868.60s	23.93s	22%	613.04s	8.10s	21%
	10	633.97s	14.48s	20%	588.64s	45.33s	32%

Table 3: Iris and HCV: each data shown for a pair (n, d) is the average of the corresponding data from five runs; nnz is percentage of the average number of non-zeros in the final solution.

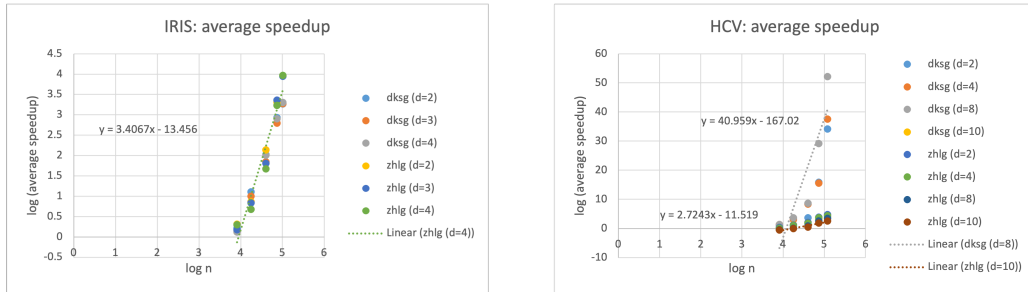


Figure 8: Average speedup of SolveNNQ over a single call of quadprog for DKSG and ZHLG.

D.2 More results on MEB

Figure 9 shows the average running times of SolveNNQ, G99, and FGK03 on 1000 nearly cospherical points. SolveNNQ overtakes G99 at $d = 20$. FGK03 is faster than SolveNNQ up to 172 dimensions; afterwards, SolveNNQ runs much faster than FGK03 as d increases.

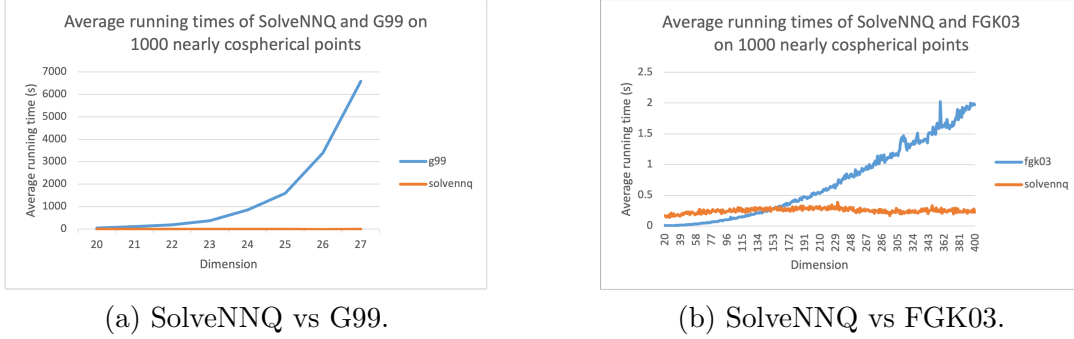


Figure 9: Average running times of SolveNNQ, G99, and FGK03 on 1000 nearly cospherical points.

D.3 Image deblurring

Let I denote a two-dimensional $r_0 \times c_0$ pixel array (an image). We call the pixel at the a -th row and b -th column the (a, b) -pixel. Let $I_{a,b}^*$ denote the intensity of the (a, b) -pixel in the original image; let $I'_{a,b}$ denote its intensity after blurring. The atmospheric turbulence point spread function determines how to distribute the intensity $I_{a,b}^*$ to other pixels [34]. At the same time, the (a, b) -pixel receives contributions from other pixels. The sum of these contributions and the remaining intensity at the (a, b) -pixel gives $I'_{a,b}$. The weight factor with respect to an (a, b) -pixel and a (c, d) -pixel is $K \cdot \exp\left(-\frac{(a-c)^2+(b-d)^2}{2\sigma^2}\right)$ for some positive constant K . It means that the contribution of the (a, b) -pixel to $I'_{c,d}$ is $K \cdot \exp\left(-\frac{(a-c)^2+(b-d)^2}{2\sigma^2}\right) \cdot I_{a,b}^*$. The point spread function is spatially invariant which makes the relation symmetric; therefore, the contribution of the (c, d) -pixel to $I'_{a,b}$ is $K \cdot \exp\left(-\frac{(a-c)^2+(b-d)^2}{2\sigma^2}\right) \cdot I_{c,d}^*$.

The atmospheric turbulence point spread function needs to be truncated as its support is infinite. We truncate it within a $(2\sigma + 1) \times (2\sigma + 1)$ square. Let B be such a $(2\sigma + 1) \times (2\sigma + 1)$ square centered at the (a, b) -pixel. It means that the (a, b) -pixel has no contribution outside B , and no pixel outside B contributes to the (a, b) -pixel. For any $s, t \in [-\sigma, \sigma]$, the weight of the entry of B at the $(a + s)$ -th row and the $(b + t)$ -th column is $K \cdot \exp\left(-\frac{s^2+t^2}{2\sigma^2}\right)$. We divide every entry of B by the total weight of all entries in B because the contributions of the (a, b) -pixel to other pixels should sum to 1. The coefficient K no longer appears in the normalized weights in B , so we do not need to worry about how to set K .

How do we transform the blurring to a multiplication of a matrix and a vector? We transpose the rows of I to columns and stack them in the row order to form a long vector \mathbf{x} . That is, the first row of I becomes the top c_0 entries of \mathbf{x} and so on. Let $M_{a,b}$ be an array with the same row and column dimensions as I . Assume for now that the square B centered at the (a, b) -entry of $M_{a,b}$ is fully contained in $M_{a,b}$. The entries of $M_{a,b}$ are zero if they are outside B ; otherwise, the entries of $M_{a,b}$ are equal to the normalized weights at the corresponding entries in B . Then, we concatenate the rows of $M_{a,b}$ in the row order to form a long row vector; this long row vector is the $((a - 1)c_0 + b)$ -th row of the matrix \mathbf{A} . The product of this $((a - 1)c_0 + b)$ -th row of \mathbf{A} and \mathbf{x} is a scalar, which is exactly the sum of the contributions of all pixels at the (a, b) -pixel, i.e., the intensity $I'_{a,b}$. Consider the case that some entries of B lie outside $M_{a,b}$. If an entry of B is outside $M_{a,b}$, we find the vertically/horizontally nearest boundary entry of $M_{a,b}$ and add to it the normalized weight at that “outside” entry of B . This ensures that the total weight within $M_{a,b}$ still sums to 1, thus making sure that no pixel intensity is lost. Afterwards, we linearize $M_{a,b}$ to form a row of \mathbf{A} as before. In all, $\mathbf{A}\mathbf{x}$ is the blurred image according to the atmospheric turbulence point spread

function.

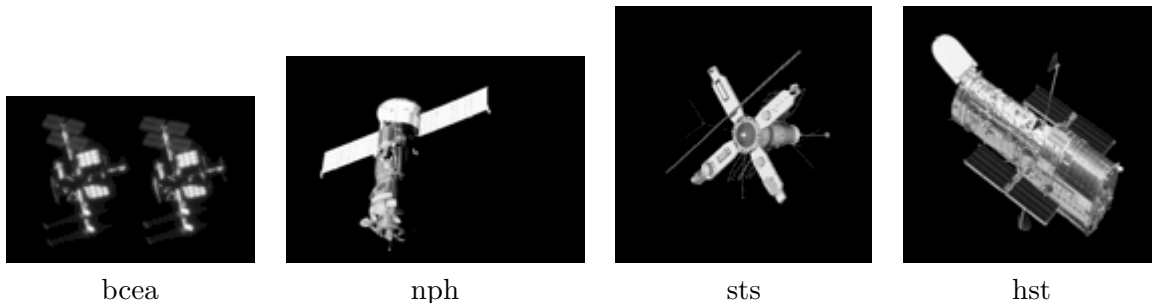


Figure 10: Four space images.

We experimented with four space images *bcea*, *nph*, *sts*, and *hst* from [2, 3, 7, 8]. We down-sample and sparsify by setting nearly black pixels (with intensities such as 10 or below, or 20 or below) to black. Figure 10 shows the four resulting space images. The image *bcea* is 124×83 ; *nph* is 149×103 ; both *sts* and *hst* are 128×128 . We generate blurred images using different values of σ .

In running SolveNNQ on the space images, we compute the gradient vector at the zero vector and select the 20τ most negative coordinates. (Recall that $\tau = 4 \ln^2 \nu$ and ν is the total number of pixels in an image in this case.) We call `quadprog` with these 20τ most negative coordinates as the only free variables and obtain the initial solution \mathbf{x}_1 . Afterwards, SolveNNQ iterates as described before. Table 2 in the main text shows the statistics of the relative mean square errors and the running times. On the next page, some blurred images are shown; the corresponding image recovered by SolveNNQ is shown below each blurred image; the value of σ used for blurring and the relative mean square error is shown between each pair of blurred and recovered images. When the relative mean square error is well below 0.01, the recovered image is visually non-distinguishable from the original.

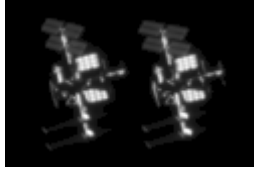
We also experimented with some thermal images *walk*, *heli*, *lion*, and *dog* [1, 4, 6]; such thermal images are typically encountered in surveillance. In each case, we extract the dominant color, down-sample, and apply thresholding to obtain a gray-scale image without most of irrelevant parts. Afterwards, we apply the uniform out-of-focus point spread function for blurring [31]—the atmospheric turbulence point spread function is not relevant in these cases. There is a positive parameter R . Given an (a, b) -pixel and a (c, d) -pixel, if $(a - c)^2 + (b - d)^2 \leq R^2$, the weight factor for them is $1/(\pi R^2)$; otherwise, the weight factor is zero. The larger R is, the blurrier is the image. The construction of the matrix \mathbf{A} works as in the atmospheric turbulence point spread function. We take a certain number of the most negative coordinates of the gradient at the zero vector, and then we call `quadprog` with these coordinates as the only free variables to obtain the initial solution \mathbf{x}_1 . Afterwards, SolveNNQ iterates as described previously.

Figure 11 shows the thermal images, the images extracted from them, the blurred images with $R = 3$, the images recovered by SolveNNQ, and the relative mean square errors (with respect to the images extracted). Table 4 shows some statistics of the experiments. All software achieve a relative mean square error well below 0.01, so their output are visually non-distinguishable from each other. In these experiments, the running times of SolveNNQ are very competitive when compared with the other software.

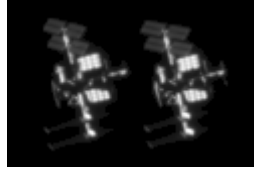
We did another experiment on deblurring the red, green, and blue color panes of a dog thermal image separately, followed by recombining the deblurred color panes. Figure 12(a) shows the original thermal image of a dog. Figures 12(b)–(d) show the gray-scale versions of the red, green, and blue pixels which have been thresholded for sparsification. Figure 12(e) shows the image obtained by



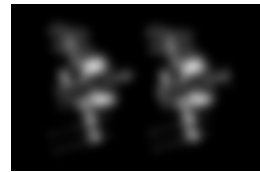
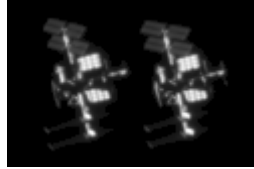
$\sigma = 1$, rel. err = 4×10^{-5}



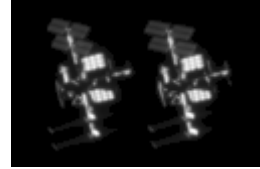
$\sigma = 1.5$, rel. err = 0.001



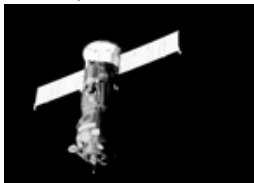
$\sigma = 2$, rel. err = 0.002



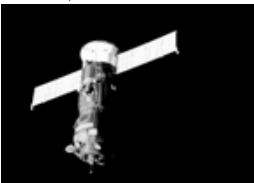
$\sigma = 2.5$, rel. err = 0.001



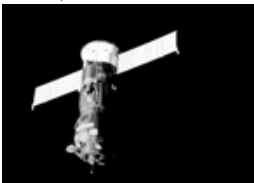
$\sigma = 1$, rel. err = 10^{-5}



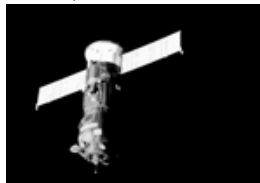
$\sigma = 1.5$, rel. err = 4×10^{-4}



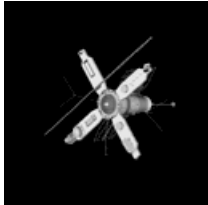
$\sigma = 2$, rel. err = 7×10^{-4}



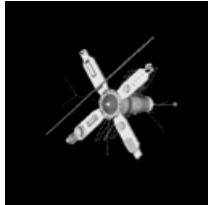
$\sigma = 2.5$, rel. err = 4×10^{-4}



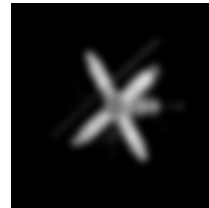
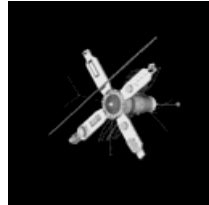
$\sigma = 1$, rel. err = 2×10^{-5}



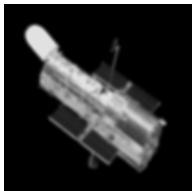
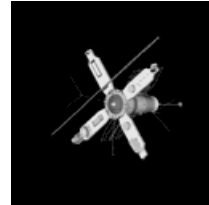
$\sigma = 1.5$, rel. err = 4×10^{-4}



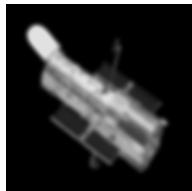
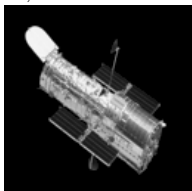
$\sigma = 2$, rel. err = 5×10^{-4}



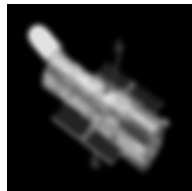
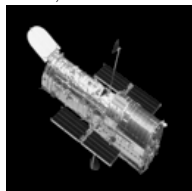
$\sigma = 2.5$, rel. err = 0.002



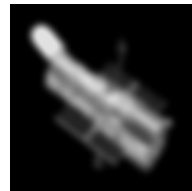
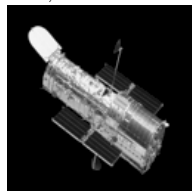
$\sigma = 1$, rel. err = 2×10^{-5}



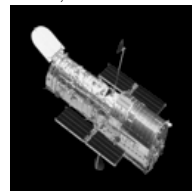
$\sigma = 1.5$, rel. err = 0.001



$\sigma = 2$, rel. err = 0.001



$\sigma = 2.5$, rel. err = 0.002



combining Figures 12(b)–(d); the result is in essence an extraction of the dog in the foreground. We blur the different color panes; Figure 13 shows these blurred color panes and their recombinations. We deblur the blurred versions of the different color panes and then recombine the deblurred color panes. The rightmost column in Figure 13 shows the recombinations of the deblurred output of SolveNNQ. As in the case of the images walk, heli, and lion, the outputs of SolveNNQ, FISTABT, SBB, FNNLS, `lsqnonneg`, and a single call `quadprog` are visually non-distinguishable from each other. Table 5 shows that the total running times of SolveNNQ over the three color panes are very competitive when compared with the other software.

Image data	R	SolveNNQ		FISTABT		SBB		FNNLS		lsqnonneg		quadprog	
		rel. err	time	rel. err	time	rel. err	time	rel. err	time	rel. err	time	rel. err	time
walk	2	6×10^{-6}	9.6s	2×10^{-11}	350s	10^{-7}	5.4s	10^{-13}	144s	4×10^{-15}	220s	6×10^{-6}	26.9s
	3	6×10^{-6}	19.1s	2×10^{-11}	1340s	2×10^{-7}	16.4s	2×10^{-13}	270s	7×10^{-15}	447s	2×10^{-5}	76.3s
	4	10^{-5}	33.1s	3×10^{-11}	2630s	2×10^{-7}	43.5s	6×10^{-13}	414s	10^{-14}	748s	10^{-5}	163s
heli	2	3×10^{-6}	1.9s	2×10^{-10}	800s	3×10^{-7}	4.9s	2×10^{-13}	57.2s	5×10^{-15}	93.8s	4×10^{-6}	12.3s
	3	2×10^{-6}	4.6s	2×10^{-10}	800s	2×10^{-7}	8.1s	5×10^{-13}	103s	10^{-14}	187s	6×10^{-6}	37.2s
	4	3×10^{-6}	8.2s	9×10^{-8}	800s	5×10^{-7}	36.8s	10^{-12}	157s	2×10^{-14}	289s	8×10^{-6}	54.7s
lion	2	10^{-6}	0.9s	6×10^{-11}	104s	6×10^{-8}	0.9s	5×10^{-14}	4.8s	3×10^{-15}	6.8s	4×10^{-6}	5.4s
	3	4×10^{-6}	1.6s	6×10^{-11}	185s	6×10^{-8}	1s	10^{-13}	8.9s	6×10^{-15}	13s	9×10^{-6}	11.7s
	4	9×10^{-6}	3.2s	5×10^{-11}	800s	2×10^{-7}	3.7s	4×10^{-13}	14.1s	10^{-14}	21.2s	7×10^{-6}	20.5s

Table 4: Results for some thermal images. In the column for each software, the number on the left is the relative mean square error, and the number on the right is the running time.

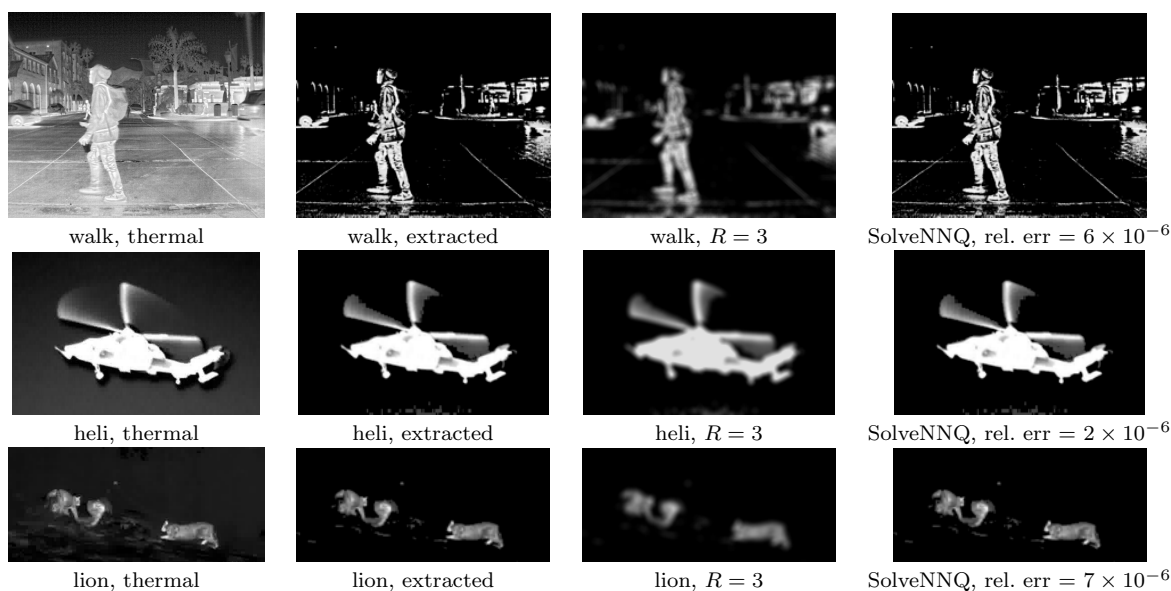


Figure 11: Thermal images.

R	SolveNNQ			FISTABT			SBB			FNNLS			lsqnonneg			quadprog		
	red	green	blue	red	green	blue	red	green	blue	red	green	blue	red	green	blue	red	green	blue
2	0.5s	0.6s	2.6s	362s	48.1s	160s	2.1s	0.7s	1.5s	4.7s	4.8s	30.6s	6.5s	6.6s	42.5s	8.7s	9.3s	10.6s
3	1s	1.3s	5.1s	663s	176s	301s	2.4s	1.3s	2.8s	8.4s	8.1s	54.1s	12.2s	11.3s	79.2s	23.1s	26.6s	30.6s
4	2s	1.9s	7.7s	800s	583s	800s	11.5s	5.5s	9.8s	14s	13.2s	78.1s	19.4s	18.6s	130s	38.6s	41.7s	42.3s

Table 5: Running times on the thresholded, blurred color panes of the dog image.

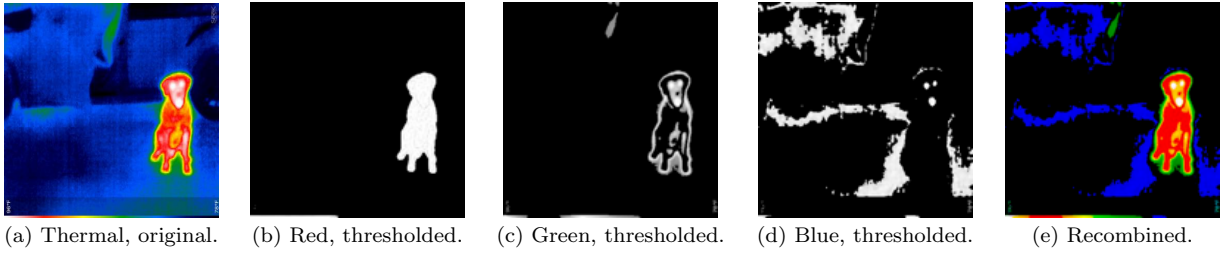


Figure 12: Thermal image of a dog, the three thresholded color panes, and their recombinations.

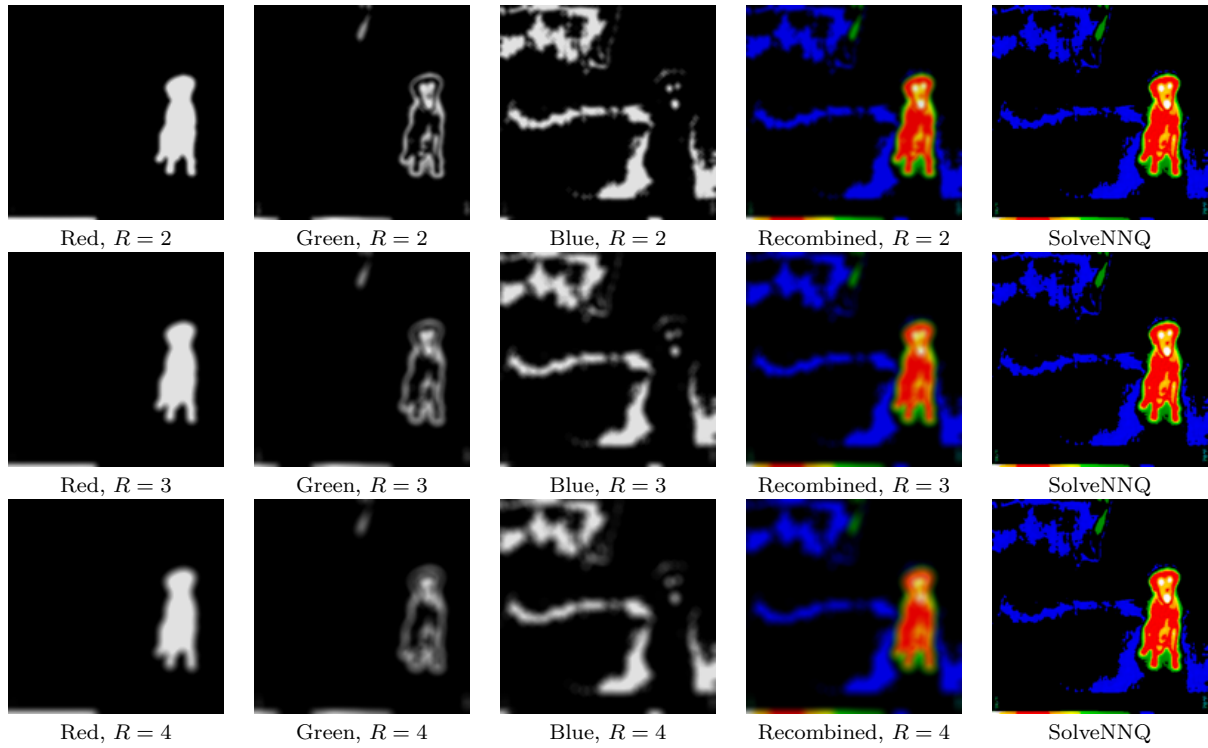


Figure 13: Blurred color panes, their recombinations, and the recombinations of the deblurred output of SolveNNQ.

D.4 The PD problem

Let $\mathbf{p}_1, \dots, \mathbf{p}_m$ and $\mathbf{q}_1, \dots, \mathbf{q}_n$ be two input point sets in \mathbb{R}^d . The PD problem is determine the distance between the convex hulls of $\mathbf{p}_1, \dots, \mathbf{p}_m$ and $\mathbf{q}_1, \dots, \mathbf{q}_n$. Wolfe [40] designed an algorithm for the special case that one of the two point sets consists of a single point; he also wrote that the problem was encountered in the optimization of non-differentiable functions, approximation theory, and pattern recognition. Sekitani and Yamamoto [36] proposed an algorithm for the general case. The PD problem is an LP-type problem [33]; it can be solved in $O(d^2n + e^{O(\sqrt{d \ln d})})$ time, but the running time increases rapidly in d . Gärtner and Schönherr [24] proposed a simplex-like algorithm for convex quadratic programming which can be used to solve the PD problem. However, it has been noted [21] that this algorithm is inefficient in high dimensions due to the use of arbitrary-precision arithmetic. The distance between the two polytopes is achieved between some convex combinations of \mathbf{p}_i 's and \mathbf{q}_j 's. In the unknown vector $\mathbf{x} \in \mathbb{R}^{m+n}$, the first m coordinates store the weights of the \mathbf{p}_i 's in their convex combination, and the last n coordinates store the weights of the \mathbf{q}_j 's in their convex combination. The constraints are $\sum_{i=1}^m (\mathbf{x})_i = 1$, $\sum_{i=m+1}^{m+n} (\mathbf{x})_i = 1$, and $\mathbf{x} \geq 0_{m+n}$. The objective function is $\mathbf{x}^t \mathbf{A}^t \mathbf{A} \mathbf{x}$, where $\mathbf{A} = [\mathbf{p}_1 \dots \mathbf{p}_m - \mathbf{q}_1 \dots - \mathbf{q}_n]$.

Our experiments are set up as follows. Let n be any fixed value. We draw $\lceil n/2 \rceil$ points uniformly at random from the d -dimensional cube $[-1, 1]^d$ to form a point set P . Similarly, we draw $\lceil n/2 \rceil$ points to form a point set Q . Then, we slide the second cube along the first axis in the positive direction so that it is at distance s from the first cube, where $s \in \{0, 4, 8\}$. Table 6 shows some average running times of SolveNNQ and a single call of `quadprog`. The average running times of `quadprog` are more or less insensitive to variations in s and d , except when $s = 0$. It seems that `quadprog` can sometimes take substantially longer time when the polytope distance is tiny; for example, when $(n, d) \in \{(2000, 100), (6000, 3), (6000, 10), (10000, 3), (10000, 10), (10000, 40)\}$. Since SolveNNQ calls `quadprog`, a similar behavior is also observed for SolveNNQ. In general, the average running time of SolveNNQ increases very slowly in d for each fixed n . Ignoring the case of $s = 0$, for each fixed d and each fixed s , the average speedup of SolveNNQ over a single call of `quadprog` is an increasing function of n . Ignoring the case of $s = 0$, for $n \geq 6000$, SolveNNQ is on average more than 5 times faster than a single call of `quadprog` for d up to 100.

		PD							
n	s	$d = 3$		$d = 10$		$d = 40$		$d = 100$	
		quadprog	ours	quadprog	ours	quadprog	ours	quadprog	ours
1000	0	0.11s	0.04s	0.10s	0.06s	0.09s	0.08s	0.10s	0.10s
	4	0.09s	0.04s	0.09s	0.04s	0.09s	0.06s	0.09s	0.06s
	8	0.10s	0.04s	0.11s	0.03s	0.10s	0.05s	0.10s	0.05s
2000	0	0.51s	0.16s	0.50s	0.19s	0.59s	0.30s	0.77s	0.38s
	4	0.50s	0.15s	0.53s	0.14s	0.63s	0.18s	0.60s	0.22s
	8	0.49s	0.14s	0.54s	0.14s	0.65s	0.18s	0.66s	0.17s
6000	0	77.95s	1.52s	10.86s	1.71s	9.27s	2.55s	9.23s	2.98s
	4	8.29s	1.34s	8.31s	1.42s	8.88s	1.77s	8.56s	1.86s
	8	8.74s	1.42s	9.26s	1.43s	9.81s	1.59s	9.78s	1.66s
10000	0	45.77s	4.71s	152.59s	5.69s	40.83s	7.69s	33.53s	9.08s
	4	33.19s	3.94s	31.80s	4.93s	34.82s	4.40s	32.26s	6.15s
	8	31.23s	3.95s	31.17s	4.18s	37.34s	4.66s	37.01s	6.04s

Table 6: Average running times of SolveNNQ and a single call of `quadprog` for the PD problem on random points from a cube. Each running time is the average over five runs.